

LINE-1 RNA triggers matrix formation in bone cells via a PKR-mediated inflammatory response

Arianna Mangiavacchi,^{1@} Gabriele Morelli,¹ Sjur Reppe,^{2,3,4} Alfonso Saera-Vila,⁵ Peng Liu,¹ Benjamin Eggerschwiler,^{6,7} Huoming Zhang,⁸ Dalila Bensaddek,⁸ Elisa A. Casanova,⁵ Carolina Medina Gomez,⁹ Vid Prijatelj,⁹ Francesco Della Valle,¹ Nazerke Atinbayeva,¹ Juan Carlos Izpisua Belmonte,¹⁰ Fernando Rivadeneira,⁹ Paolo Cinelli,^{5,11} Kaare Morten Gautvik,^{3*} Valerio Orlando.^{1*@}

¹ King Abdullah University of Science and Technology (KAUST), Biological Environmental Science and Engineering Division, Thuwal 23500-6900, Kingdom of Saudi Arabia

² Oslo University Hospital, Department of Medical Biochemistry, Oslo, Norway.

³Lovisenberg Diaconal Hospital, Unger-Vetlesen Institute, Oslo, Norway.

⁴Oslo University Hospital, Department of Plastic and Reconstructive Surgery, Oslo, Norway.

⁵ Sequentia Biotech, Carrer Comte D'Urgell 240, Barcelona, 08036, Spain.

⁶Department of Trauma, University Hospital Zurich, Sternwartstrasse 14, 8091, Zurich, Switzerland

⁷ Life Science Zurich Graduate School, University of Zurich, Winterthurerstrasse 190, 8057, Zurich, Switzerland.

⁸ Core Labs, King Abdullah University of Science and Technology (KAUST), Thuwal 23500-6900, Kingdom of Saudi Arabia.

⁹ Department of Internal Medicine, Erasmus Medical Centre, Rotterdam, the Netherlands.

¹⁰ Altos Labs, San Diego, CA, USA

¹¹ Center for Applied Biotechnology and Molecular Medicine, University of Zurich, Winterthurerstrasse 190, 8057, Zurich, Switzerland.

*senior author

@corresponding author

Abstract

Transposable elements (TEs) are mobile genetic modules of viral derivation that have been co-opted to become modulators of mammalian gene expression. TEs are a major source of endogenous dsRNAs, signaling molecules able to coordinate inflammatory responses in various physiological processes. Here, we provide evidence for a

positive involvement of TEs in inflammation-driven bone repair and mineralization. In newly fractured mice bone, we observed an early transient upregulation of repeats occurring concurrently with the initiation of the inflammatory stage. In human bone biopsies, analysis revealed a significant correlation between repeats expression, mechanical stress and bone mineral density. We investigated a potential link between LINE-1 (L1) expression and bone mineralization by delivering a synthetic L1 RNA to osteoporotic patient-derived mesenchymal stem cells and observed a dsRNA-triggered protein kinase (PKR)-mediated stress response that led to strongly increased mineralization. This response was associated with a strong and transient inflammation, accompanied by a global translation attenuation induced by eIF2 α phosphorylation. We demonstrated that L1 transfection reshaped the secretory profile of osteoblasts, triggering a paracrine activity that stimulated the mineralization of recipient cells.

Keywords: dsRNA/inflammation/osteoblast /PKR/transposable elements

Introduction

Repetitive elements are, in origin, parasitic transposable elements (TEs) of viral derivation and during evolution have become regulatory modules of gene expression, eventually integrated into developmental, resilience, and cell identity programs.(Cosby *et al*, 2019) (Mangiavacchi *et al*, 2021) (Jachowicz *et al*, 2017) Although cells have evolved several defense mechanisms to prevent deleterious uncontrolled retrotransposon reactivation,(Slotkin & Martienssen, 2007) increasing evidence demonstrates that retrotransposons are also involved in non-pathological contexts, particularly as non-coding RNAs.(Mangiavacchi *et al*, 2021) As part of resilience mechanisms, all retrotransposons are a major source of endogenous double-stranded RNAs (dsRNAs), that serve as a cellular signaling molecule to coordinate inflammatory and immune responses in various physiological processes.(Fukuda *et al*, 2021) (De Cecco *et al*, 2019a) (Simon *et al*, 2019) (Sadeq *et al*, 2021) (Chen & Hur, 2022) (Zhang *et al*, 2020) The transient and controlled breaching of the activation threshold of dsRNA sensors allows the integration of innate immune functions within the frame of physiological processes.(Chen & Hur, 2022) For example, repetitive elements transcribed during development drive RIG-I-like receptors (RLR)-mediated inflammatory signals that regulate hematopoietic stem and progenitor cells (HSPC) formation.(Lefkopoulos *et al*, 2020) During cell replication, dsRNA-mediated activation of PKR ensures proper progression of mitosis.(Kim *et al*, 2014) Moreover, epigenetically mediated derepression of repetitive elements leads to dsRNA production and to the activation of an

inflammatory response stimulating anti-tumor T cell immunity.(Sheng *et al*, 2018) Furthermore, after skin injury, dsRNAs induce inflammatory pathways contributing to wound healing and hair regeneration.(Nelson *et al*, 2015) Several studies have demonstrated a positive effect of proinflammatory mediators on bone anabolism *in vitro* and *in vivo*,(Croes *et al*, 2015) (Croes *et al*, 2016) (Li *et al*, 2016) (Croes *et al*, 2017) (Laroche *et al*, 2011) suggesting that an inflammatory reaction may be harnessed for bone regenerative purposes. Indeed, sterile inflammation is a fundamental component of the osteogenic microenvironment: the inflammatory reaction is the earliest response to injury and is crucial to initiate and orchestrate fracture repair and activate bone anabolic processes. (Mountziaris *et al*, 2011) (Marsell & Einhorn, 2011) (Bahney *et al*, 2019) Accordingly, a dysregulated inflammation negatively impacts optimal bone regeneration, (Wheatley *et al*, 2019) (Gerstenfeld *et al*, 2001) (Recknagel *et al*, 2013) (Hurtgen *et al*, 2016) (Jiao *et al*, 2015) and often precedes the excessive bone formation associated with heterotopic ossification and several vertebral column pathological conditions. (Lories & Schett, 2012) (Balboni *et al*, 2006) Therefore, identifying the key molecular factors triggering the sterile inflammation that precedes regeneration in bone would allow us to modulate the inflammatory reaction in a spatiotemporal and contextual manner as well as to develop new anabolic strategies for the treatment of bone loss conditions, such as osteoporosis, or impaired bone repair.(Roberts & Ke, 2018)

Here, we show that 1) In mice, immediately after bone fracture, a transient upregulation of TEs concurs with the initiation of the inflammatory stage; 2) in humans, an increased expression of repeats is observed in bones with a higher mechanical stress-induced anabolic demand and expression of TEs correlates with local mineral density; 3) The delivery of L1 RNA, but not control RNA, to human bone marrow-derived mesenchymal stem cells committed to osteoblasts stimulates a unique mineralizing phenotype in a dose-dependent manner; 4) L1-treated osteoblasts show upregulation of inflammatory genes and transcriptional changes characteristic for the earliest stage of bone repair; 5) cytoplasmic L1 RNA is sensed by dsRNA-activated protein kinase (PKR), which mediates eIF2 α phosphorylation and a global attenuation of protein synthesis; 6) the inhibition of PKR prevents inflammation, inhibits translation and induces mineralization caused by elevated levels of cytoplasmic L1 RNA; 7) cells transfected with L1 RNA undergo significant changes in their secretome composition and initiate a paracrine effect stimulating the mineralization of osteogenic competent recipient cells.

Our results indicate that TEs are induced by bone damage and stimulate bone mineralization through an inflammatory response triggered by dsRNA sensing and mediated by a paracrine activity.

Results

Retrotransposon expression is triggered by fracture *in vivo* and correlates with bone mineral density in human weight-bearing bones

Inflammation is the earliest response in fracture healing. To investigate a possible involvement of TEs in the sterile inflammatory response triggered by bone injury, we analyzed TEs expression in time-course RNA-Seq repository data obtained from a full-fracture bone healing mice model.(Coates *et al*, 2019) We focused on TEs expression dynamics immediately after fracture (acute inflammatory stage) and observed four clusters of differentially expressed TEs ($\log_{2}FC > 0.5$) between intact and post-fracture bone after 4h, a time point corresponding to the initiation of acute inflammation (Figure 1A). Cluster 1 includes TEs subfamilies whose expression slightly increases after fracture and during the whole healing process. Clusters 2 and 4 include TEs subfamilies that are downregulated after fracture but show increased expression at later time points. The major group, cluster 3, is represented by TEs subfamilies whose expression is highly and transiently upregulated after fracture (Figure 1A and 1B). Interestingly, the induction of these TEs, mostly Long Interspersed Nuclear Elements (LINEs) and Long Terminal Repeats (LTRs) (Figure 1B), is transient and limited to the earliest phase of the inflammatory stage necessary and sufficient to initiate and orchestrate fracture repair and activate bone anabolic processes.(Mountziaris *et al*, 2011)(Marsell & Einhorn, 2011) These results suggest that, in bone, retrotransposon reactivation is an early event in response to fracture, possibly linked to inflammation initiation which is fundamental for a healthy healing. Indeed, retrotransposon involvement in posttraumatic tissue regeneration was previously found in other organisms.(Mashanov *et al*, 2012)(Zhu *et al*, 2012)

To assess gene expression dynamics immediately after fracture in humans represents a technical and ethical hurdle. A comparison between bones experiencing different degrees of mechanical loading may represent an alternative model to study stress-induced bone anabolism in humans. Mechanically loaded bones like the femur, which are subject to recurring microfractures that need to be repaired, are indicated to be more metabolically active than less loaded bones, like the iliac crest, as pointed out by previous transcriptome studies.(Aerssens *et al*, 1997) (Varanasi *et al*, 2010)

We compared the expression of TEs in trabecular bone from ilium and femoral head, two different skeletal sites, the latter experiencing a higher degree of mechanical loading, anabolic demand and bone turnover.(Aerssens *et al*,

1997) Femur (n=48) and ilium biopsies (n=71) were isolated from a cohort of clinically well-characterized donors (refer to cohort description and Appendix Table S1 and S2). Each cohort was divided into normal (BMD T-score > 1), osteopenic ($-2.5 < \text{BMD T-score} \leq -1$), and osteoporotic (BMD T-score ≤ -2.5 , with at least one fragility fracture). TEs show generally higher upregulation in healthy femurs (n=27) compared to healthy ilia (n=34) (Figure 1C and 1E). Each TEs order showed a high percentage of upregulated subfamilies, from 60% of DNA transposon to 75% of LINEs, and a low percentage of downregulated subfamilies, from 9% of LTRs to 3% of Short interspersed nuclear elements (SINEs) and LINEs, in femur compared to ilium (Figure 1D). These results suggested a positive correlation between TEs global expression and bone anabolic activity.

To further test our hypothesis, we compared TEs expression in femurs from healthy donors (n=27), osteopenic (n=12) and osteoporotic patients (n=9) whose bone anabolism is increasingly compromised. As shown in Figure 2A, the global expression of TEs is reduced in patients. To further assess whether TEs expression is involved in local anabolism and associated with mineral density, we divided the femur cohort according to the DXA T-score measured in the femoral neck (FN). We divided the cohort into “high BMD” (FN T-score >-1) and “low BMD” (FN T-score <-1). Globally, TEs are upregulated in femurs with high bone mineral density (Figure 2B). In particular, more than 90% of differentially expressed TEs subfamilies are upregulated (Figure 2C). Interestingly, almost all SINE elements are unchanged between the two groups (Figure 2C). Finally, we assessed whether a positive correlation exists between TEs expression levels and local mineral density (FN T-score). We found that approximately 30% of L1 and LTR subfamilies expressed in the femoral bone are positively correlated with local BMD (Figure 2D). Altogether, these results strongly suggest a positive involvement of TEs in response to stress-induced anabolic demand and bone mineralization.

Increased cytoplasmic L1 repeat RNA stimulates osteoblast mineralization activity

The *in vivo* evidence suggested a positive involvement of retrotransposons in post-traumatic bone repair in mice, and a strong correlation between retrotransposon expression and bone mineral density in humans, and higher expression in loaded compared to unloaded bone. We then corroborated the results by studying the effects of increasing repeat RNA levels on differentiating osteoblasts derived from mesenchymal stem cells (MSCs) isolated from femurs of healthy donors. At day 5 of differentiation, a Cy5-conjugated full-length L1 RNA consensus sequence was transfected. Capping, 2'-O-Methylation of 5' end, polyadenylation (200 adenosines), full substitution with 5-

methylcytidine (m5C) and 75% substitution with pseudouridine were used to stabilize the RNA and to bypass the intracellular innate immune system.(Koski *et al*, 2004) (Pardi *et al*, 2013) (Ludwig *et al*, 2010) (Karikó *et al*, 2005) (Nallagatla & Bevilacqua, 2008) (Karikó *et al*, 2008) (Anderson *et al*, 2010) (Kormann *et al*, 2011) Red fluorescent protein (RFP) mRNA, with the same modifications, was included as negative control. The exogenous L1 RNA accumulated in the cytoplasm (Figure 3A) and was gradually cleared by secretion along with matrix components (Figure 3B and 3C). The effect of L1 RNA delivery was tested in differentiating MSCs from two different and unrelated healthy donors. As shown, L1 RNA transfection markedly stimulated the production of mineralized matrix (Figure 3D). Osteoblast mineralization increased dose-dependently with the concentration of the delivered L1 RNA, in agreement with saturation kinetics (Figure 3E). Moreover, the strongly enhanced mineralization was highly specific for L1 RNA, as demonstrated by the lack of significant changes in mineral deposition in cells transfected with negative control RNA, even at concentrations 100-200-fold higher (figure 3E). We also isolated MSCs from the femur of osteoporotic patients and selected those showing a markedly delayed and reduced *in vitro* production of bone matrix in contrast to those derived from healthy donors (Figure 3F). Strikingly, also in these cells with low osteogenic capacity, the delivery of L1 RNA triggered a strong mineralization response despite their clearly compromised anabolic activity (Figure 3G). These results demonstrate convincingly that the ectopic delivery of L1 RNA stimulates the mineralization of bone-forming cells regardless of their prior intrinsic differentiation/anabolic potential.

Osteoporotic patient-derived cells transfected with L1 RNA show a higher expression of early differentiation markers, with a peak 48h after L1 transfection (day 7) (Figure 3H). Bone sialoprotein (*IBSP*), a late osteogenic gene, shows a similar profile, being almost 6 times more expressed in L1- than in RFP-transfected cells on day 7 (Appendix Figure S1A). Strikingly, although alkaline phosphatase (*ALPL*) expression slightly increases at later time points (Appendix Figure S1A), its activity is not enhanced in L1-treated cells (Appendix Figure S2A). However, the activity of ectonucleotide pyrophosphatase/phosphodiesterase 1 (ENPP1) is gradually and significantly reduced by L1 RNA transfection (Appendix Figure S2B). As ENPP1 is a major source of inorganic pyrophosphate (PPi), one of the main physiological inhibitors of mineralization,(FLEISCH *et al*, 1966) (Johnson *et al*, 2000) (Hessle *et al*, 2002) the reduction of its activity may contribute to the enhanced mineralization observed in L1-RNA transfected cells. Altogether, these data suggest that L1 RNA induces a unique mineralizing phenotype and apparently distinct from the well-known canonical differentiation mechanisms.

L1 RNA delivery induces inflammatory pathways significantly overlapping those involved in bone fracture repair

To investigate the molecular response of osteoblasts to L1 RNA transfection, we profiled their transcriptome by Illumina RNA-Seq 24h post-transfection. We found 482 differentially expressed genes (DEG) (FDR<0.05) between L1 and RFP RNA-treated OB (268 upregulated and 214 downregulated) (Appendix Figure S3). Gene ontology (GO) enrichment analysis revealed that the early transcriptional signature of L1-treated osteoblasts is typical of that of an inflammatory response (Figure 4A and 4B). This is in accordance with the recent evidence of a link between L1 and other retrotransposons accumulation in the cytoplasm and inflammatory response *in vitro* and *in vivo*. (Fukuda *et al*, 2021) (De Cecco *et al*, 2019b) (Simon *et al*, 2019) GO term enrichment analysis comparison between the early stage of fracture-induced bone healing *in vivo* (Coates *et al*, 2019) and differentiating osteoblasts *in vitro* 24h post-L1 delivery (Figure 4A) revealed a matching inflammatory response and shared upregulated pathways (Figure 4C) essential for effective bone repair. (Maruyama *et al*, 2020) (Gerstenfeld *et al*, 2003) (Kon *et al*, 2001) Recruitment of neutrophils at the site of injury also indicates a healthy repair process, particularly in bone. (Kovtun *et al*, 2016) Extracellular signal-regulated kinase 1 (ERK1) and 2 (ERK2), play crucial roles in bone formation (Xiao *et al*, 2000) (Xiao *et al*, 2002b) (Xiao *et al*, 2002a) (Matsushita *et al*, 2009) (Ge *et al*, 2007) and seem to be the most upstream initiators of tissue regeneration in planaria. (Owlarn *et al*, 2017) Upon bone injury, an initial transient stage of acute inflammation is a crucial factor in ensuring an effective regeneration (Maruyama *et al*, 2020) whereas an excessive/prolonged (chronic) inflammation is deleterious for the healing environment. (Chan *et al*, 2012) (Hurtgen *et al*, 2016) (Clark *et al*, 2017) (Brem & Tomic-Canic, 2007) (Timmen *et al*, 2014) (Schmidt-Bleek *et al*, 2012) (Weckbach *et al*, 2013) We followed the time-course expression of “inflammatory response” (GO:0006954) and “immune response” (GO:0006955) genes upregulated by L1 RNA immediately after transfection. As shown in Figure 4D, their expression is already strongly reduced at day 10 and almost entirely silenced by day 14, suggesting the transient dynamics of the inflammatory response triggered *in vitro* by L1 RNA. This is coherent with our previous observation that exogenous L1 RNA is gradually secreted by the cell together with matrix components (Figure 3B and C), eventually clearing out the initial inflammatory stimulus.

Cellular response to increased cytoplasmic level of L1 RNA is mediated by PKR

It has been previously demonstrated that the cytoplasmic accumulation of L1-derived cDNA triggers an inflammatory response mediated by the cyclic GMP-AMP synthase (cGAS)-stimulator of interferon genes (STING) cytosolic DNA sensing pathway.(De Cecco *et al*, 2019a) Immunofluorescence (IF) analysis reveals that the exogenous L1 RNA forms DNA:RNA hybrids (Appendix Figure S4), suggesting that L1 RNA is reversed transcribed into cDNA after its transfection. Notably, ORF1p was undetectable by WB in differentiating osteoblasts and in L1 transfected osteoblasts (Appendix Figure S5), indicating that the exogenous L1 RNA is not translated after transfection. To assess whether L1-induced inflammation was triggered by the sensing of its cDNA, we used Lamivudine 3TC and G140 (Figure 5A) to inhibit the ORF2-mediated reverse transcription of L1 RNA and cGAS activity, respectively. Moreover, we also performed a siRNA-mediated knockdown (KD) of cGAS (Appendix Figure S6). (Jones *et al*, 2008) (Lama *et al*, 2019) Surprisingly, none of the treatments impaired the mineralization induced by L1 RNA delivery (Figure 5A, Appendix Figure S6C), suggesting that the observed cellular response depends entirely on RNA sensing. As previously mentioned, repeats are a major source of endogenous dsRNA,(Sadeq *et al*, 2021) (Chen & Hur, 2022) and L1 RNA, in particular, is able to form intramolecular double-stranded structures.(Hur, 2019) As expected, we found a tight colocalization between L1 RNA and dsRNA IF signal (Figure 5B). One of the main cellular sensors of dsRNA, including those derived from retrotransposons, is PKR.(Kim *et al*, 2018) PKR activation results in the phosphorylation of eukaryotic translation initiation factor 2 α (eIF2 α) and in the subsequent inhibition of global protein synthesis and cell growth.(Donnelly *et al*, 2013) Interestingly, PKR has been shown to interact with L1 RNA *in vitro*.(Kim *et al*, 2018) Moreover, eIF2 α phosphorylation has been demonstrated to promote autophagy in osteoblasts and to counteract BMD reduction in osteoporotic ovariectomized mice.(Li *et al*, 2019)

To demonstrate that L1 RNA is able to trigger a PKR-mediated intracellular response, we transfected L1 RNA in the presence or absence of the PKR inhibitor C16 and evaluated the levels of eIF2 α phosphorylation by western blot (Figure 5C). The delivery of L1, but not RFP, strongly induces eIF2 α phosphorylation and this effect is prevented by PKR inhibition (Figure 5C). Notably, eIF2 α phosphorylation occurs already 6 hours post-transfection. This observation suggests that PKR activation is one of the first events induced by L1 RNA, thus corroborating the hypothesis of PKR as an endogenous L1 RNA sensor.

We then characterized the proteome of cells 24h post-L1 RNA transfection by diaPASEF mass spectrometry (MS).(Meier *et al*, 2020a) We detected almost 8000 proteins in each sample, and observed that more than 88% of

significantly differentially expressed proteins (DEP) were downregulated in L1-treated cells (Figure 5D, left panel). Moreover, among the top 15 downregulated biological processes and cellular components were translation and ribosomal subunits (Figure 5D, right panels, yellow circles), indicating that L1 RNA induces a global attenuation of protein synthesis. Indeed, a cap-dependent translation shutdown is the main consequence of eIF2 α phosphorylation.(Donnelly *et al*, 2013) Finally, we show that neither PKR KD (Appendix Figure S6A, B) nor its pharmacological inhibition by C16 treatment (Figure 5E and 5F) prevents L1 RNA-triggered induction of inflammatory genes (Figure 5E) and mineral matrix deposition (Figure 5F, Appendix Figure S6B). As previously mentioned, a global reduction of protein synthesis occurs 24h after L1 transfection and only a little percentage of DEP is upregulated in L1 compared to RFP control (Figure 5D). Interestingly, some of the most upregulated proteins are involved in autophagy and vesicle trafficking (Figure 5G). Autophagy is a crucial process for mineralization and bone homeostasis both *in vitro* and *in vivo*,(Nollet *et al*, 2014) as autophagic vacuoles are exploited to secrete apatite crystals.

Altogether these data demonstrate that the PKR-mediated sensing of L1-derived dsRNA globally attenuates the translation via eIF2 α phosphorylation and indicate autophagy as a possible mechanism involved in L1-induced osteoblasts mineralization.

L1 RNA delivery reshapes the secretory profile of differentiating osteoblasts

An inflammatory response translates into a strong secretory activity and production of paracrine signals, and we therefore tested the effect of “L1-primed” osteoblast-derived conditioned medium in recipient differentiating osteoblasts (Figure 6A). We found that the “secretome” of cells transfected with L1 RNA has a significant paracrine effect on recipient osteoblasts since they showed an earlier formation of mineralized nodules, already 24h post the addition of conditioned media (Figure 6A, right panel), and higher deposition of mineral matrix at day 10 (Figure 6A, left panel). We subsequently isolated bulk and exosome-derived proteomes from conditioned media of untreated, RFP- and L1-treated differentiating osteoblasts and characterized them by MS. Differential expression analysis of MS data revealed a unique secretome profile (for both bulk and vesicular proteomes) of L1-primed osteoblasts compared to RFP-primed and untreated osteoblasts (Figure 6B). Gene Ontology (GO) analysis of differentially expressed proteins showed an enrichment of pro-inflammatory factors (i.e. interleukins and chemokines) involved in immune response and chemotactic migration of immune cells (Figure 6C and D), crucial

processes for tissue repair mechanisms *in vivo*. Pro-inflammatory molecules are also a major constituent of the senescence-associated secretory phenotype (SASP),(Coppé *et al*, 2010) whose transient delivery supports cellular plasticity and tissue regeneration.(Ritschka *et al*, 2017) Notably, the most enriched protein in L1-specific bulk secretome is interleukin 8 (IL-8), an inflammatory chemokine involved in several regenerative processes, such as skin wound healing,(JIANG *et al*, 2012) therapeutic angiogenesis after stroke and ischemia,(Choi *et al*, 2021) (Hou *et al*, 2014) and osteochondral bone repair.(Lin *et al*, 2019) (Yang *et al*, 2018a) Tumor necrosis factor-inducible gene 6 (TSG6) is among the top 10 proteins enriched in the bulk secretome of L1-primed osteoblasts compared to RFP. TSG6 is an inflammatory factor with suggestive therapeutic effects in corneal wounds, myocardial infarction, injured central nervous system, chronic liver damage, and intervertebral disc degeneration.(Zhang *et al*, 2013) (Lee *et al*, 2015) (Lee *et al*, 2009) (Wang *et al*, 2017) (Yang *et al*, 2018b) Moreover, TSG6 induces autophagy influx both *in vivo* and *in vitro*.(Wang *et al*, 2017) Another protein positively involved in autophagy and found specifically in the secretome of L1 primed osteoblasts was ATG7 (autophagy-related 7). Osteoblast-specific ATG7 conditional knockout in mice reduced bone mass during developmental and in adult age.(Li *et al*, 2018) Type 1 lysophosphatidic acid receptor (LPAR1) is also specifically secreted by L1-primed osteoblasts and has proven to be positively involved in bone mineralization *in vitro* and *in vivo*.(Alioli *et al*, 2020) (Gennero *et al*, 2011)

Altogether, our findings demonstrate that cytoplasmic L1 RNA is sensed by PKR, whose activation leads to eIF2 α phosphorylation with consequent reprogramming of transcription and translation. The ultimate consequence of this L1-induced, PKR-mediated stress response in osteoblasts is a major reprogramming of their secretory activity, leading to a paracrine effect on recipient osteogenic competent cells to trigger their mineralization activity.

Discussion

The concerted co-option of TEs markedly changed whole regulatory networks and integrated new functions into the eukaryote genome.(Cosby *et al*, 2019) (Mangiavacchi *et al*, 2021) (Carelli *et al*, 2022) However, while the role of TEs as evolutionary drivers is today well-established, their contribution to cell physiology, particularly in somatic cells, remains to be elucidated. Indeed, aside from their role in the nucleus, (Della Valle *et al*, 2022) (Jachowicz *et al*, 2017) (Lu *et al*, 2021) (Percharde *et al*, 2018) TEs represent a major source of endogenous dsRNA whose role in triggering inflammatory and innate immune responses in various physiological processes has increasingly gained attention.(Sadeq *et al*, 2021) (Chen & Hur, 2022) For instance, an early acute inflammatory response is of vital

importance in initiating and orchestrating bone repair and induce anabolism leading to fracture healing. (Mountziaris *et al*, 2011) (Marsell & Einhorn, 2011) (Bahney *et al*, 2019) Moreover, several studies demonstrated a positive effect of proinflammatory mediators on bone mineralization *in vitro* and *in vivo*,(Croes *et al*, 2015) (Croes *et al*, 2016) (Li *et al*, 2016) (Croes *et al*, 2017) indicating that the modulation of inflammatory reaction is a tool to pursue regenerative strategies in bone.(Roberts & Ke, 2018) We found that, in the bone of newly fractured mice, a group of TEs, mostly LINE and LTR, was early, markedly and transiently upregulated. Interestingly, the expression of these TEs was limited to the earliest phase of the inflammatory stage. In line with the hypothesis of a positive correlation between stress-induced bone mineralization and TEs activation, the expression dynamics in human bone biopsies revealed a significant upregulation of TEs in the femur, a bone subjected to high mechanical stresses, high turnover and anabolism, compared to ilium, not weight bearing. Furthermore, we detected a lower TEs expression in donors with compromised bone mineralization and a significant correlation between TEs expression and local BMD. We hypothesized that the expression dynamics of TEs in fracture/mechanical stress observed *in vivo* could mimic the immunological threshold model of the sterile activation of dsRNA sensors as a response to stressful conditions. Indeed, the transient and controlled breaching of the activation threshold of dsRNA sensors may lead to sterile inflammation being integrated into physiological processes.(Chen & Hur, 2022) To test further this hypothesis, we delivered a full-length L1 consensus sequence as source of dsRNA(Hur, 2019) to differentiating osteoblasts *in vitro* and showed that L1 RNA initially accumulated in the cytoplasm and is gradually cleared by secretion. The increased cytoplasmic levels of L1 RNA are immediately sensed by PKR, a cytoplasmic dsRNA sensor whose activation induces the phosphorylation of eIF2 α (Kιμ $\varepsilon\tau \alpha\lambda$, 2018) ($\Delta\text{οννελλψ} \varepsilon\tau \alpha\lambda$, 2013), leading to the attenuation of global protein synthesis (Donnelly *et al*, 2013), induction of inflammatory response, and stimulation of mineral matrix deposition. In support of the evidence that PKR is the early sensor of increased L1 RNA cytoplasmic levels, we show that inhibition of PKR activation by C16 prevents L1-induced eIF2 α phosphorylation, induction of inflammatory genes, and mineral matrix deposition. Moreover, the inhibition of L1 cDNA formation and sensing by Lamivudine 3TC, G140, or cGAS KD does not affect the L1-induced phenotype. Thus, the evidence does not support that the L1-triggered inflammation is causally connected to a cGAS-STING-dependent sensing of cytosolic L1 cDNA, a mechanism demonstrated operative in senescence.(De Cecco *et al*, 2019a)

L1 RNA response showed high specificity, as demonstrated by the dose-dependent increase of mineralization and the lack of significant changes in mineral deposition when negative control RNA was transfected, even at 100-200-

fold higher concentration. Although the molecular mechanism behind L1-induced stress response which stimulates the mineralization activity of osteoblasts remains elusive, our results indicate that L1 stimulates the mineral matrix deposition by bone-forming cells regardless of their prior intrinsic anabolic potential. Moreover, MS results suggested that increased autophagy, a process crucial for mineralization and bone homeostasis *in vitro* and *in vivo*(Nollet *et al*, 2014) may contribute to L1-induced hydroxyapatite deposition. Intriguingly, the osteoinductive properties of L1-primed osteoblast-derived secretome and the observation that L1 RNA was gradually secreted by the cells may suggest an involvement of L1 RNA in cell-to-cell communication, in line with the recent finding of other retrotransposons (i.e. ERV) acting as paracrine molecules.(Liu *et al*, 2021) This, together with the observed L1-dependent induction of CCL and CXCL chemokines and cytokines, being chemoattractants of immune cells and endothelial cells,(Bischoff *et al*, 2011) (Eash *et al*, 2010) (Strieter *et al*, 2005) and the composition of L1-primed osteoblast secretome, makes the *in vivo* delivery of L1 RNA a necessary step to evaluate its actual contribution to the paracrine processes that orchestrate bone repair mechanisms. (Chaparro & Linero, 2016) (Nimiritsky *et al*, 2019) The identification of repeats RNA, particularly L1, as potential resilient molecular factors involved in stress-induced, inflammation-mediated bone production points out new avenues to develop anabolic strategies for the treatment of bone loss conditions, such as osteoporosis or impaired bone repair.(Roberts & Ke, 2018) On the other hand, repeats may be novel targets in the treatment of those conditions characterized by excessive or heterotopic ossification preceded by deregulated/chronic inflammation.(Lories & Schett, 2012) (Balboni *et al*, 2006)

Materials and Methods

Participants and ethics

Femoral bone biopsies were obtained from the caput region of postmenopausal women or men with a wide BMD range, i.e., from healthy to osteoporotic, who were undergoing hip replacement surgery due to osteoarthritis or fracture at Lovisenberg Diaconal Hospital (Oslo, Norway) or Diakonhjemmet Hospital (Oslo, Norway), respectively. The donors of femoral bones are listed in Appendix Table S1. The postmenopausal iliac bone donors were recruited from the outpatient clinic of Lovisenberg Diaconal Hospital (Oslo, Norway). Candidates filled out a questionnaire that included medication and lifestyle factors, and selected donors were deemed representative of the Oslo-based Norwegian ethnic female population aged 50 to 86 years. The iliac bone donors are listed in Appendix Table S2 and have been described previously in detail.(Reppe *et al*, 2010) All donors taking medication or having

diseases, other than primary osteoporosis, known to affect bone metabolism were excluded. The presence of bone-impairing diseases/conditions was excluded by extensive biochemical serum and urine analyses supported by X-ray examinations. The site-specific BMD of all donors was evaluated with Lunar Prodigy DEXA (GE Lunar, Madison, WI, USA) following the manufacturer's instructions. The precision of the instrument for measuring the lumbar spine (L_2-L_4) and hip BMD was 1.7% and 1.1%, respectively. The study was approved by the Norwegian Regional Ethical Committee (REK no 2010/2539, Norway), all volunteers gave their written informed consent, and sampling and procedures were according to the Act of Biobanking in Norway.

Cell culture

For L1 RNA transfection experiments, human MSCs were isolated from osteoporotic femoral heads with the consent of the patient according to Swiss (BASEC-Nr. 2016-02159) ethical guidelines. Femoral heads were crushed and incubated in DMEM (PAN Biotech, Germany, Cat. No. P04-03550) supplemented with 1% (v/v) 100× Penicillin-Streptomycin Solution (Biowest, France, Cat. No. L0022), 10% (v/v) FCS (Biowest, France, Cat. No. S181S), 1% (v/v) 200mM L-Glutamine solution (Sigma, USA, Cat. No. G7513), 5ng/ml FGF-2 (Sigma, USA, Cat. No. F0291) and 10ng/ml FGF-4 (Sigma, USA, Cat. No. F8424) in a humidified atmosphere containing 5% CO₂. To induce osteogenic differentiation, MSCs were seeded on Nunc™ 24-well plates (Thermo Fisher, USA, Cat. No. 142475) or 48-well plates (Thermo Fisher, USA, Cat. No. 150687) at a density of 1.5×10^4 cells/cm². After 24 h, differentiation was induced using StemPro® Osteogenesis Kit (Gibco/Life Technologies, USA, Cat. No. A10072-01). The medium was exchanged every 3 days. Cells were treated with Lamivudine 3TC (Sigma), 1μM final concentration; C16 (Merck), 500nM final concentration; G140 (InvivoGen), 150μM final concentration.

L1 RNA transfection

The vector human-L1_pBluescript II sk (+) carrying the full-length L1 sequence was custom-prepared by GenScript, USA. Large-scale human L1 mRNA was in vitro transcribed, modified, and purified by TriLink Biotechnologies, USA, (ARCA capped and 2'Omethylated (CapI), fully substituted with 5-methyl-C, 25% substitution of Cyanine-5-U and 75% substitution of Pseudo-U, enzymatically polyadenylated, DNase and phosphatase treated, silica membrane purified). Synthetic L1 RNA was transfected in MSCs differentiating to osteoblasts at day 5 using Lipofectamine™ MessengerMAX™ (Invitrogen, USA, Cat. No. LMRNA003) with a modified protocol for low RNA amount. RFP mRNA (System Bioscience, USA, Cat. No. MR800A-1) was used as negative control. Bone matrix was quantified with OsteoImage Mineralization Assay (Lonza, Basel, Switzerland, Cat. No. LOPA503) and

Alizarin Red staining. In conditioned media experiments, the medium was exchanged 6h after transfection. Conditioned medium was collected after three days and delivered to the recipient, differentiating osteoblasts at day 5. In knockdown experiments, siRNAs were transfected with Lipofectamine RNAiMAX (Thermo Scientific) in differentiating osteoblasts at day 3, followed by L1 RNA transfection at day 7. siRNAs: EIF2AK2- Targeting SMARTpool (Dharmacon, Horizon, E-003527-00-0010), MB21D1-Targeting SMARTpool (Dharmacon, Horizon, L-015607-02-0020), Non-targeting Pool (D-001810-10).

Quantitative mineralization assay

Cells were washed in PBS and fixed in 4% (v/v) formaldehyde (Sigma, USA, Cat. No. F8775) in 1× PBS for 15 minutes. Mineralization was assessed by using the OsteoImage Mineralization Assay (Lonza, Basel, Switzerland, Cat. No. LOPA503) according to the manufacturer's indication. Mineralization was quantified with GloMax® discover microplate reader (Promega, USA), selecting appropriate excitation (492) / emission (520) wavelengths.

Alizarin Red staining

Osteoblasts were washed with 1× PBS (Kantonsapotheke Zürich, Switzerland, Cat. No. A171012) and fixed with 4% (v/v) formaldehyde (Sigma, USA, Cat. No. F8775) in 1× PBS for 30 min. After washing twice with ddH₂O, Alizarin Red staining solution (0.7 g Alizarin Red S (Sigma, USA, Cat. No. A5533) diluted in 50 ml ddH₂O at pH = 4.2) was added for 20 min. Afterwards, cells were washed four times with ddH₂O, dried, and stored in the dark until image acquisition. For absorbance measurement, Alizarin Red S was eluted from stained osteoblasts with 300 µl 10% (w/v) cetylpyridinium chloride in an aqueous 0.01 M Na₂HPO₄/NaH₂PO₄ solution at pH = 7 for 1 h. One hundred fifty microliters were transferred on a 96-well plate, and absorbance was measured at 560 nm. Ten percent (w/v) cetylpyridinium chloride in an aqueous 0.01 M Na₂HPO₄/NaH₂PO₄ solution was used as blank. Images were acquired, processed and analysed as previously described(Eggerschwiler *et al*, 2019)

ALPL activity assay:

ALPL activity was measured as in Liu et al., 2016.(Liu *et al*, 2016) Briefly, cells were fixed in 3.7% formaldehyde at RT for 10' and then stained with a solution of 25% naphthol AS-BI phosphate (Thermo) and 0.75% Fast Blue BB (Sigma) dissolved in 0.1 M Tris buffer (pH 9.3) at RT for 15'. After staining, cells were quickly washed with PBS five times.

ENPP1 activity assay

ENPP1 activity was calculated colorimetrically using the chromogenic substrate p-nitrophenyl-thymidine-5'-monophosphate, as described in (Ferreira et al., 2013). After PBS washing, cells were lysed in a solution of 0.1% Triton X-100, 0.2 M Tris-base, 1.6 mM MgCl₂, pH 8.1. 50 µl of 1mM thymidine monophosphate p-nitrophenyl ester (Sigma) were added to 50 µl of cell lysate and incubated for 1 hour at 37°C. Then, four volumes of 0.1M NaOH were added to stop the reaction and absorbance was read at 410 nm using a spectrophotometer (Tecan Nanoquant Infinite 200 Pro Multimode). Absorbance was normalized to DNA content.

Immunohistochemistry:

Cells were fixed in 4% paraformaldehyde in PBS at room temperature (RT) for 10'. After fixation, cells were permeabilized in 3% Triton X-100 in PBS for 3' at RT. Blocking was performed with 4% BSA in PBS for 30' at RT. After blocking, cells were incubated with primary antibodies overnight at 4°C, then washed with PBS and incubated with secondary antibodies for 1 hour at RT. After washing with PBS, nuclei were stained with Hoechst (Thermo Scientific) and mounted using Fluoro Gel with DABCO™ Mounting Medium (Electron Microscopy Sciences). Primary antibodies: DNA-RNA Hybrid (mouse, Merck Millipore, MABE1095), dsRNA (mouse, Merck Millipore, MABE1134).

RNA extraction and cDNA preparation

Cells were harvested and resuspended in 1ml of QIAzol Lysis reagent (Qiagen, Cat. No.79306). Total RNA was then purified with RNeasy Plus Mini kit (Qiagen, cat. No. 74134) with minimal modifications to manufacturer's instructions. DNase treatment (RNase-free DNase set, Qiagen, Cat. No. 79254) was performed to remove any residual DNA. RNA quality and concentration were checked using a Nanodrop™ 2000 spectrophotometer (ThermoFisher). cDNA was synthesized from 200ng of each RNA sample using a Superscript III first-strand cDNA synthesis system (ThermoFisher, cat. No.18080051) according to the manufacturer's protocol. Processing of human bone biopsies and RNA isolation has been described previously.(Reppe *et al*, 2010)

Gene expression analysis

Real-time quantitative polymerase chain reaction (qPCR) was performed with a 7900HT Fast Real-Time PCR system (Applied Biosystems). Each sample was analyzed in triplicate and normalized with the endogenous control Ribosomal Protein L13A (*RPL13A*) for cDNA input concentration. No template and no RT were included as negative controls. For each 15µl reaction, 10ng (1ng for L1) of cDNA was mixed with 1µM specific primers mix and 7.5µl of Sybr™ Select Master mix (Applied Biosystems, USA, Cat. No. 4472908). The reaction was incubated

at 95°C for 10 minutes, followed by 40 cycles of denaturation at 95°C for 15 seconds, annealing at 60°C for 30 seconds and elongation at 72°C for 30 seconds. Ct values were calculated by 7900HT Fast Real-Time PCR RQ manager software (Applied Biosystems, USA) and then normalized as ΔCt between the gene of interest and the endogenous calibrator. Primers used in this study for gene expression analysis were designed using Primer3 (<http://www.ncbi.nlm.nih.gov/tools/primer-blast/>). In all primer pairs, each primer matches a different exon. Amplicons length was 80-130 nucleotides. Primer sequences are reported in Appendix Table S3.

Cell cycle analysis

2x10⁵ MSCs were trypsinized for 5 min at 37°C, washed with PBS and 2% BSA, passed through a 70μM strainer (Corning, USA, Cat. No. 352350) and then fixed at -20°C for 30 min in 70% ethanol. After washing with PBS and 4% BSA, cells were resuspended in PBS and incubated for 1 hour at 37°C with RNase. Cells were then washed and resuspended in 100μl of Flow Cytometry Staining Buffer (R&D System, USA, Cat. No. FC001). 10μl of 1mg/ml Propidium iodide (PI) staining solution (Invitrogen, USA, Cat. No. P3566) was added to the single-cell solution, gently mixed, and incubated for 5 min in the dark. Cell cycle analysis was performed on BD FACSCanto II Flow Cytometry System (BD-Biosciences), using BD FACSDiva Software (BD-Biosciences).

RNA-Seq and data analysis

RNA from human bone biopsies was sequenced at the Human Genotyping facility (HuGe-F) of Erasmus MC. Total RNA-Seq library, from L1 RNA delivery experiments, was prepared with CORALL Total RNA library prep with RiboCop rRNA for Human/Mouse/Rat depletion kit (Lexogen GmbH, Vienna, Austria) following manufacturer's instructions (library type: fr-secondstrand) by IGA Technology service (Italy). The final libraries were checked using both Qubit 2.0 Fluorometer (Invitrogen, Carlsbad, CA) and Agilent Bioanalyzer DNA assay or Caliper (PerkinElmer, Waltham, MA). Libraries were then prepared for sequencing and sequenced on paired-end 150 bp mode on NovaSeq6000 (Illumina, San Diego, CA). RNA-Seq read quality control (QC) analyses and filtering of high-quality reads were executed using FastQC v0.11.9 (<http://www.bioinformatics.babraham.ac.uk/projects/fastqc/>) and BBduk v35.85 (<https://jgi.doe.gov/data-and-tools/software-tools/bbtools/bb-tools-user-guide/bbduk-guide/>) by setting a minimum read length of 35 bp and a minimum Phred-quality score of 25. After trimming quality control, high-quality reads were aligned to the human genome reference (GRCh38) with STAR 2.7.3a,(Dobin *et al*, 2013) while FeatureCounts 1.6.3 package(Liao *et al*, 2014) was used to assign reads to genes. Next, lowly expressed genes across one or more experimental conditions

were filtered to eliminate the “uninformative” genes using HTSFilter v1.30.1.(Rau *et al*, 2013) Filtered gene data were further processed with the EdgeR package v3.32.1(Robinson *et al*, 2010) to normalize (Trimmed Mean of M-7 values, TMM, method) the raw counts and perform differential gene expression analysis. Multiple testing correction was performed with the FDR method(Benjamini & Hochberg, 1995) and significance level was set at FDR < 0.05. Gene Ontology (GO) term enrichment was analyzed by performing hypergeometric tests¹¹ for each individual term, and FDR correction was applied (FDR < 0.05). Expression of Interspersed Repeat elements was quantified using SQuIRE 0.9.9.92 (<https://github.com/wyang17/SQuIRE>). SQuIRE provides locus-specific expression quantification along with subfamily-level expression estimates counting unambiguously mapped reads, as well as ambiguously mapped reads using an expectation–maximization (EM) algorithm.(Yang *et al*, 2019) Briefly, reference genome and Repeatmasker annotation were downloaded from UCSC and prepared for the analysis with squire Fetch and squire Clean, respectively. High-quality reads were mapped against the reference genome with STAR using squire Map and expression was quantified using squire Call. Differential expression analysis was performed with squire Call.

DIA-MS analysis using TimsTOF MS

Total protein extracts were prepared with RIPA buffer (50mMTris-cl pH 8.0, 5mM EDTA, 150mM Nacl, 15mM MgCl₂, 1% NP-40, 1mM PMSF and 1X Protease Inhibitor Cocktail (PIC)). Further sonication step was included: (30S ON, 30S OFF, 10 cycles with Bioruptor). Equal 50 µg protein extracts were concentrated to 30 µl volume, then diluted in 8M urea in 0.1M Tris-HCl, followed by protein digestion with trypsin, according to the FASP protocol.(Wiśniewski *et al*, 2009) After overnight digestion, the peptides were eluted from the filters with 25 mM ammonium bicarbonate buffer. The eluted peptides were processed in the desalting step using Sep-Pag C18 Column (waters) based on the manufacturer’s instructions. Approximately 200 ng of peptide mixture per sample was analyzed using a timsTOF Pro 2 QTOF mass spectrometer coupled with a nanoElute liquid chromatography system (Bruker Daltonik GmbH, Germany). The sample was injected directly into an RP-C18 Aurora emitter column (75 µm i.d.× 250 mm, 1.6 µm, 120 Å pore size) (Ion Opticks, Australia) using a one-column separation method. An 80-min gradient was established using mobile phase A (0.1% FA in H₂O) and mobile phase B (0.1% FA in Acetonitrile): 2–25% B for 60 min, 25–37% for 10 min, ramping 37% to 95% in 5 min, and maintaining 95% B for 5 min. The column temperature was set at 50°C and the flow rate at 250 nl/min. The sample eluting from the separation column was introduced into the mass spectrometer via a CaptiveSpray nano-electrospray ion source (Bruker Daltonik GmbH) with an electrospray voltage of 1.6 kV. The ion source temperature was set to 180 °C and a

dry gas of 3 l/min. The samples were analyzed using diaPASEF scheme(Meier *et al*, 2020b) consisting of 24 cycles including a total of 48 mass width windows (13 Da (m/z) from m/z 400 to 1,000 and TIMS scan range from 0.63 to 1.35 Vs cm⁻² (1/K0). The collisional energy increased linearly from 20.01 eV at 0.6 (1/K0) to 52.00 eV at 1.35 Vs cm⁻² (1/K0). The scan range for MS and MS/MS spectra was set to 100-1700 m/z. TIMS ramping time and accumulation time were set to 100 milliseconds. The diaPASEF data were analyzed by directDIA approach using Spectronaut software (version 14) following manufacture instructions. Up or down regulated proteins were determined using DEP (Differential Enrichment analysis of Proteomics data) R package. Significant results (adjusted p-value < 0.05) were subjected to Gene Ontology enrichment analysis with clusterProfiler R package.

Western Blot

Total protein extracts were prepared by lysing cells in extraction buffer (HEPES KOH [pH 8.5], NaCl 400 mM, EDTA 0.1 mM, EGTA 0.1 mM, DTT 1 mM, 1× protease inhibitor, SDS 1%). Proteins were separated by electrophoresis on BOLT 4%–12% bis-tris polyacrylamide precast gels in MES buffer (Life Technologies) and transferred to a 0,2 µm nitrocellulose membrane. Non-specific signals were blocked with 5% Milk-PBS-Tween0.5% and the membrane hybridized overnight at 4°C with primary and secondary antibodies diluted in blocking buffer. Horseradish peroxidase-conjugated secondary antibodies were revealed with the ECL chemiluminescence kit (Amersham), and signals were detected using ChemiDoc (Bio-Rad). Primary antibodies: PKR (rabbit, Abcam, ab32052), cGAS (rabbit, Abcam, ab224144), LINE-1 ORF1 (mouse, Merck Millipore, MABC1152), EIF2a (mouse, Abcam, ab5369), phospho-EIF2α (rabbit, Abcam, ab32157), Histone H3 (rabbit, Merk, 06-755).

Exosome isolation

Exosomes were isolated using Total Exosome Isolation Reagent (from cell culture media) (Thermo), following manufacturer's instructions. The exosome pellet was resuspended in 50 µl of RIPA buffer and kept on ice for 30', mixing every 5'. Samples were then sonicated (30'' ON/30'' OFF, 10 cycles), centrifuged at 13,000 x g for 20' at 4°C and collected as supernatants.

Statistical analysis

Statistic tests used for data analysis are indicated in the figure legends.

Data availability

The RNA-seq transcriptomics data on human bone biopsies have been deposited to BioProject with the dataset identifier PRJNA764663 (<https://www.ncbi.nlm.nih.gov/bioproject/PRJNA764663>). The RNA-seq transcriptomics

data on transfected osteoblasts have been deposited to GEO with the dataset identifier GSE201774 (<https://www.ncbi.nlm.nih.gov/geo/query/acc.cgi?acc=GSE201774>) (enter token: ififogaehzoxlgh).

The mass spectrometry proteomics data have been deposited to the ProteomeXchange Consortium via the PRIDE partner repository with the dataset identifier PXD051195. Reviewer account details are username: reviewer_pxd051195@ebi.ac.uk; password: R6v0mIYe

Acknowledgment

We acknowledge kaust Smarth Health Initiative (KSHI); the South-Eastern Norway Regional Health Authority; the Norwegian Osteoporosis Society; Anders Jahre Foundation for the Promotion of Science; the Lovisenberg Diaconal Hospital research fund; and the Research Council of Norway.

Funding: We are grateful for support from: KAUST BAS/1/1037-01-01, the European Union project OSTEOPHENE (no. FP6-502491); ZonMw VIDI 016.136.367 grant, for funding the creation of the RNA-Seq dataset of hip primary bone and Oslo University Hospital, Ullevål, project #29750104.

Disclosure and competing interests statement: All the authors declare no competing interests.

References

- Aerssens J, Boonen S, Joly J & Dequeker J (1997) Variations in trabecular bone composition with anatomical site and age: potential implications for bone quality assessment. *J Endocrinol* 155: 411–421
- Alioli CA, Demesmay L, Laurencin-Dalacieux S, Beton N, Farlay D, Follet H, Saber A, Duboeuf F, Chun J, Rivera R, et al (2020) Expression of the type 1 lysophosphatidic acid receptor in osteoblastic cell lineage controls both bone mineralization and osteocyte specification. *Biochim Biophys Acta - Mol Cell Biol Lipids* 1865: 158715
- Anderson BR, Muramatsu H, Nallagatla SR, Bevilacqua PC, Sansing LH, Weissman D & Karikó K (2010) Incorporation of pseudouridine into mRNA enhances translation by diminishing PKR activation. *Nucleic Acids Res*

- Bahney CS, Zondervan RL, Allison P, Theologis A, Ashley JW, Ahn J, Miclau T, Marcucio RS & Hankenson KD (2019) Cellular biology of fracture healing. *J Orthop Res* 37: 35–50
- Balboni TA, Gobezie R & Mamon HJ (2006) Heterotopic ossification: Pathophysiology, clinical features, and the role of radiotherapy for prophylaxis. *Int J Radiat Oncol* 65: 1289–1299
- Benjamini Y & Hochberg Y (1995) Controlling the False Discovery Rate: A Practical and Powerful Approach to Multiple Testing. *J R Stat Soc Ser B* 57: 289–300
- Bischoff DS, Sakamoto T, Ishida K, Makhijani NS, Gruber HE & Yamaguchi DT (2011) CXC receptor knockout mice: characterization of skeletal features and membranous bone healing in the adult mouse. *Bone* 48: 267–274
- Brem H & Tomic-Canic M (2007) Cellular and molecular basis of wound healing in diabetes. *J Clin Invest* 117: 1219–1222
- Carelli FN, Cerrato C, Dong Y, Appert A, Dernburg A & Ahringer J (2022) Widespread transposon co-option in the *Caenorhabditis* germline regulatory network. *Sci Adv* 8
- De Cecco M, Ito T, Petraschen AP, Elias AE, Skvir NJ, Criscione SW, Caligiana A, Brocculi G, Adney EM, Boeke JD, et al (2019a) L1 drives IFN in senescent cells and promotes age-associated inflammation. *Nature* 566: 73–78
- De Cecco M, Ito T, Petraschen AP, Elias AE, Skvir NJ, Criscione SW, Caligiana A, Brocculi G, Adney EM, Boeke JD, et al (2019b) L1 drives IFN in senescent cells and promotes age-associated inflammation. *Nature* 566: 73–78
- Chan JK, Roth J, Oppenheim JJ, Tracey KJ, Vogl T, Feldmann M, Horwood N & Nanchahal J (2012) Alarmins: awaiting a clinical response. *J Clin Invest* 122: 2711
- Chaparro O & Linero I (2016) Regenerative Medicine: A New Paradigm in Bone Regeneration. In *Advanced Techniques in Bone Regeneration* InTech
- Chen YG & Hur S (2022) Cellular origins of dsRNA, their recognition and consequences. *Nat Rev Mol Cell Biol* 23: 286–301
- Choi J, Choi W, Joo Y, Chung H, Kim D, Oh SJ & Kim S-H (2021) FGF2-primed 3D spheroids producing IL-8 promote therapeutic angiogenesis in murine hindlimb ischemia. *NPJ Regen Med* 6: 48
- Clark D, Nakamura M, Miclau T & Marcucio R (2017) Effects of Aging on Fracture Healing. *Curr Osteoporos Rep*

- Coates BA, McKenzie JA, Buettmann EG, Liu X, Gontarz PM, Zhang B & Silva MJ (2019) Transcriptional Profiling of Intramembranous and Endochondral Ossification after Fracture in Mice. *Bone* 127: 577
- Coppé J-P, Desprez P-Y, Krtolica A & Campisi J (2010) The Senescence-Associated Secretory Phenotype: The Dark Side of Tumor Suppression. *Annu Rev Pathol Mech Dis* 5: 99–118
- Cosby RL, Chang NC & Feschotte C (2019) Host-transposon interactions: conflict, cooperation, and cooption. *Genes Dev* 33: 1098–1116
- Croes M, Boot W, Kruyt MC, Weinans H, Pouran B, van der Helm YJM, Gawlitta D, Vogely HC, Alblas J, Dhert WJA, et al (2017) Inflammation-Induced Osteogenesis in a Rabbit Tibia Model. *Tissue Eng Part C Methods* 23: 673–685
- Croes M, Öner FC, Kruyt MC, Blokhuis TJ, Bastian O, Dhert WJA & Alblas J (2015) Proinflammatory Mediators Enhance the Osteogenesis of Human Mesenchymal Stem Cells after Lineage Commitment. *PLoS One* 10: e0132781
- Croes M, Öner FC, van Neerven D, Sabir E, Kruyt MC, Blokhuis TJ, Dhert WJA & Alblas J (2016) Proinflammatory T cells and IL-17 stimulate osteoblast differentiation. *Bone* 84: 262–270
- Dobin A, Davis CA, Schlesinger F, Drenkow J, Zaleski C, Jha S, Batut P, Chaisson M & Gingeras TR (2013) STAR: ultrafast universal RNA-seq aligner. *Bioinformatics* 29: 15–21
- Donnelly N, Gorman AM, Gupta S & Samali A (2013) The eIF2 α kinases: their structures and functions. *Cell Mol Life Sci* 70: 3493–3511
- Eash KJ, Greenbaum AM, Gopalan PK & Link DC (2010) CXCR2 and CXCR4 antagonistically regulate neutrophil trafficking from murine bone marrow. *J Clin Invest* 120: 2423–2431
- Eggerschwiler B, Canepa DD, Pape HC, Casanova EA & Cinelli P (2019) Automated digital image quantification of histological staining for the analysis of the trilineage differentiation potential of mesenchymal stem cells. *Stem Cell Res Ther*
- FLEISCH H, RUSSELL RGG & STRAUMANN F (1966) Effect of Pyrophosphate on Hydroxyapatite and Its Implications in Calcium Homeostasis. *Nature* 212: 901–903
- Fukuda S, Varshney A, Fowler BJ, Wang S Bin, Narendran S, Ambati K, Yasuma T, Magagnoli J, Leung H, Hirahara S, et al (2021) Cytoplasmic synthesis of endogenous Alu complementary DNA via reverse

- transcription and implications in age-related macular degeneration. *Proc Natl Acad Sci U S A* 118
- Ge C, Xiao G, Jiang D & Franceschi RT (2007) Critical role of the extracellular signal-regulated kinase–MAPK pathway in osteoblast differentiation and skeletal development. *J Cell Biol* 176: 709
- Gennero I, Laurencin-Dalicieux S, Conte-Auriol F, Briand-Mésange F, Laurencin D, Rue J, Beton N, Malet N, Mus M, Tokumura A, *et al* (2011) Absence of the lysophosphatidic acid receptor LPA1 results in abnormal bone development and decreased bone mass. *Bone* 49: 395–403
- Gerstenfeld LC, Cho T-J, Kon T, Aizawa T, Cruceta J, Graves BD & Einhorn TA (2001) Impaired Intramembranous Bone Formation during Bone Repair in the Absence of Tumor Necrosis Factor-Alpha Signaling. *Cells Tissues Organs* 169: 285–294
- Gerstenfeld LC, Cullinane DM, Barnes GL, Graves DT & Einhorn TA (2003) Fracture healing as a post-natal developmental process: Molecular, spatial, and temporal aspects of its regulation. *J Cell Biochem* 88: 873–884
- Hessle L, Johnson KA, Anderson HC, Narisawa S, Sali A, Goding JW, Terkeltaub R & Millan JL (2002) Tissue-nonspecific alkaline phosphatase and plasma cell membrane glycoprotein-1 are central antagonistic regulators of bone mineralization. *Proc Natl Acad Sci U S A* 99: 9445–9
- Hou Y, Ryu CH, Jun JA, Kim SM, Jeong CH & Jeun S (2014) IL-8 enhances the angiogenic potential of human bone marrow mesenchymal stem cells by increasing vascular endothelial growth factor. *Cell Biol Int* 38: 1050–9
- Hur S (2019) Double-Stranded RNA Sensors and Modulators in Innate Immunity. *Annu Rev Immunol* 37: 349–375
- Hurtgen BJ, Ward CL, Garg K, Pollot BE, Goldma SM, McKinley TO, Wenke JC & Corona BT (2016) Severe muscle trauma triggers heightened and prolonged local musculoskeletal inflammation and impairs adjacent tibia fracture healing. *J Musculoskelet Neuronat Interact* 16: 122
- Jachowicz JW, Bing X, Pontabry J, Bošković A, Rando OJ & Torres-Padilla ME (2017) LINE-1 activation after fertilization regulates global chromatin accessibility in the early mouse embryo. *Nat Genet*
- JIANG WG, SANDERS AJ, RUGE F & HARDING KG (2012) Influence of interleukin-8 (IL-8) and IL-8 receptors on the migration of human keratinocytes, the role of PLC- γ and potential clinical implications. *Exp Ther Med* 3: 231–236
- Jiao H, Xiao E & Graves DT (2015) Diabetes and Its Effect on Bone and Fracture Healing. *Curr Osteoporos Rep* 13: 327–335

- Johnson KA, Hessle L, Vaingankar S, Wennberg C, Mauro S, Narisawa S, Goding JW, Sano K, Millan JL & Terkeltaub R (2000) Osteoblast tissue-nonspecific alkaline phosphatase antagonizes and regulates PC-1. *Am J Physiol Regul Integr Comp Physiol* 279: R1365-77
- Jones RB, Garrison KE, Wong JC, Duan EH, Nixon DF & Ostrowski MA (2008) Nucleoside analogue reverse transcriptase inhibitors differentially inhibit human LINE-1 retrotransposition. *PLoS One*
- Karikó K, Buckstein M, Ni H & Weissman D (2005) Suppression of RNA recognition by Toll-like receptors: The impact of nucleoside modification and the evolutionary origin of RNA. *Immunity*
- Karikó K, Muramatsu H, Welsh FA, Ludwig J, Kato H, Akira S & Weissman D (2008) Incorporation of pseudouridine into mRNA yields superior nonimmunogenic vector with increased translational capacity and biological stability. *Mol Ther*
- Kim Y, Lee JH, Park J-E, Cho J, Yi H & Kim VN (2014) PKR is activated by cellular dsRNAs during mitosis and acts as a mitotic regulator. *Genes Dev* 28: 1310–1322
- Kim Y, Park J, Kim S, Kim MA, Kang MG, Kwak C, Kang M, Kim B, Rhee HW & Kim VN (2018) PKR Senses Nuclear and Mitochondrial Signals by Interacting with Endogenous Double-Stranded RNAs. *Mol Cell* 71: 1051-1063.e6
- Kon T, Cho TJ, Aizawa T, Yamazaki M, Nooh N, Graves D, Gerstenfeld LC & Einhorn TA (2001) Expression of osteoprotegerin, receptor activator of NF- κ B ligand (osteoprotegerin ligand) and related proinflammatory cytokines during fracture healing. *J Bone Miner Res* 16: 1004–1014
- Kormann MSD, Hasenpusch G, Aneja MK, Nica G, Flemmer AW, Herber-Jonat S, Huppmann M, Mays LE, Illenyi M, Schams A, et al (2011) Expression of therapeutic proteins after delivery of chemically modified mRNA in mice. *Nat Biotechnol*
- Koski GK, Karikó K, Xu S, Weissman D, Cohen PA & Czerniecki BJ (2004) Cutting Edge: Innate Immune System Discriminates between RNA Containing Bacterial versus Eukaryotic Structural Features That Prime for High-Level IL-12 Secretion by Dendritic Cells. *J Immunol*
- Kovtun A, Bergdolt S, Wiegner R, Radermacher P, Huber-Lang M & Ignatius A (2016) The crucial role of neutrophil granulocytes in bone fracture healing. *Eur Cells Mater* 32: 152–162
- Lama L, Adura C, Xie W, Tomita D, Kamei T, Kuryavyi V, Gogakos T, Steinberg JI, Miller M, Ramos-Espiritu L, et al (2019) Development of human cGAS-specific small-molecule inhibitors for repression of dsDNA-

- triggered interferon expression. *Nat Commun* 10: 2261
- Laroche M, Livideanu C, Paul C & Cantagrel A (2011) Interferon Alpha and Pamidronate in Osteoporosis with Fracture Secondary to Mastocytosis. *Am J Med* 124: 776–778
- Lee MJ, Kim DH, Ryu JS, Ko AY, Ko JH, Kim MK, Wee WR, Khwarg SI & Oh JY (2015) Topical TSG-6 Administration Protects the Ocular Surface in Two Mouse Models of Inflammation-Related Dry Eye. *Invest Ophthalmol Vis Sci* 56: 5175–81
- Lee RH, Pulin AA, Seo MJ, Kota DJ, Ylostalo J, Larson BL, Semprun-Prieto L, Delafontaine P & Prockop DJ (2009) Intravenous hMSCs improve myocardial infarction in mice because cells embolized in lung are activated to secrete the anti-inflammatory protein TSG-6. *Cell Stem Cell* 5: 54–63
- Lefkopoulos S, Polyzou A, Derecka M, Bergo V, Clapes T, Cauchy P, Jerez-Longres C, Onishi-Seebacher M, Yin N, Martagon-Calderón N-A, et al (2020) Repetitive Elements Trigger RIG-I-like Receptor Signaling that Regulates the Emergence of Hematopoietic Stem and Progenitor Cells. *Immunity* 53: 934–951.e9
- Li C, Li G, Liu M, Zhou T & Zhou H (2016) Paracrine effect of inflammatory cytokine-activated bone marrow mesenchymal stem cells and its role in osteoblast function. *J Biosci Bioeng* 121: 213–219
- Li H, Li D, Ma Z, Qian Z, Kang X, Jin X, Li F, Wang X, Chen Q, Sun H, et al (2018) Defective autophagy in osteoblasts induces endoplasmic reticulum stress and causes remarkable bone loss. *Autophagy* 14: 1726–1741
- Li J, Li X, Liu D, Hamamura K, Wan Q, Na S, Yokota H & Zhang P (2019) eIF2 α signaling regulates autophagy of osteoblasts and the development of osteoclasts in OVX mice. *Cell Death Dis* 10: 921
- Liao Y, Smyth GK & Shi W (2014) featureCounts: an efficient general purpose program for assigning sequence reads to genomic features. *Bioinformatics* 30: 923–930
- Lin D, Chai Y, Ma Y, Duan B, Yuan Y & Liu C (2019) Rapid initiation of guided bone regeneration driven by spatiotemporal delivery of IL-8 and BMP-2 from hierarchical MBG-based scaffold. *Biomaterials* 196: 122–137
- Liu W, Zhou L, Zhou C, Zhang S, Jing J, Xie L, Sun N, Duan X, Jing W, Liang X, et al (2016) GDF11 decreases bone mass by stimulating osteoclastogenesis and inhibiting osteoblast differentiation. *Nat Commun* 7: 12794
- Liu X, Liu Z, Sun L, Ren J, Wu Z, Jiang X, Ji Q, Wang Q, Fan Y, Cai Y, et al (2021) Resurrection of human endogenous retroviruses during aging reinforces senescence. *bioRxiv*
- Lories RJU & Schett G (2012) Pathophysiology of New Bone Formation and Ankylosis in Spondyloarthritis. *Rheum*

Dis Clin North Am 38: 555–567

- Lu JY, Chang L, Li T, Wang T, Yin Y, Zhan G, Han X, Zhang K, Tao Y, Percharde M, *et al* (2021) Homotypic clustering of L1 and B1/Alu repeats compartmentalizes the 3D genome. *Cell Res* 31: 613–630
- Ludwig J, Schuberth C, Goldeck M, Schlee M, Li H, Juranek S, Sheng G, Micura R, Tuschl T, Hartmann G, *et al* (2010) Structural and functional insights into 5'-PPP RNA pattern recognition by the innate immune receptor RIG-I. *Nat Struct Mol Biol*
- Mangiavacchi A, Liu P, Della Valle F & Orlando V (2021) New insights into the functional role of retrotransposon dynamics in mammalian somatic cells. *Cell Mol Life Sci* 78: 5245–5256
- Marsell R & Einhorn TA (2011) The biology of fracture healing. *Injury* 42: 551–555
- Maruyama M, Rhee C, Utsunomiya T, Zhang N, Ueno M, Yao Z & Goodman SB (2020) Modulation of the Inflammatory Response and Bone Healing. *Front Endocrinol (Lausanne)* 11: 386
- Mashanov VS, Zueva OR & García-Arrarás JE (2012) Posttraumatic regeneration involves differential expression of long terminal repeat (LTR) retrotransposons. *Dev Dyn* 241: 1625–1636
- Matsushita T, Chan YY, Kawanami A, Balmes G, Landreth GE & Murakami S (2009) Extracellular signal-regulated kinase 1 (ERK1) and ERK2 play essential roles in osteoblast differentiation and in supporting osteoclastogenesis. *Mol Cell Biol* 29: 5843–5857
- Meier F, Brunner AD, Frank M, Ha A, Bludau I, Voytik E, Kaspar-Schoenfeld S, Lubeck M, Raether O, Bache N, *et al* (2020a) diaPASEF: parallel accumulation-serial fragmentation combined with data-independent acquisition. *Nat Methods* 17: 1229–1236
- Meier F, Brunner AD, Frank M, Ha A, Bludau I, Voytik E, Kaspar-Schoenfeld S, Lubeck M, Raether O, Bache N, *et al* (2020b) diaPASEF: parallel accumulation-serial fragmentation combined with data-independent acquisition. *Nat Methods* 17: 1229–1236
- Mountzaris PM, Spicer PP, Kasper FK & Mikos AG (2011) Harnessing and Modulating Inflammation in Strategies for Bone Regeneration. *Tissue Eng Part B Rev* 17: 393
- Nallagatla SR & Bevilacqua PC (2008) Nucleoside modifications modulate activation of the protein kinase PKR in an RNA structure-specific manner. *RNA*
- Nelson AM, Reddy SK, Ratliff TS, Hossain MZ, Katseff AS, Zhu AS, Chang E, Resnik SR, Page C, Kim D, *et al* (2015) dsRNA Released by Tissue Damage Activates TLR3 to Drive Skin Regeneration. *Cell Stem Cell* 17:

- Nimiritsky P, Eremichev R, Alexandrushkina N, Efimenko A, Tkachuk V & Makarevich P (2019) Unveiling Mesenchymal Stromal Cells' Organizing Function in Regeneration. *Int J Mol Sci* 20: 823
- Nollet M, Santucci-Darmanin S, Breuil V, Al-Sahlanee R, Cros C, Topi M, Momier D, Samson M, Pagnotta S, Cailleteau L, et al (2014) Autophagy in osteoblasts is involved in mineralization and bone homeostasis. *Autophagy* 10: 1965–1977
- Owlarn S, Klenner F, Schmidt D, Rabert F, Tomasso A, Reuter H, Mulaw MA, Moritz S, Gentile L, Weidinger G, et al (2017) Generic wound signals initiate regeneration in missing-tissue contexts. *Nat Commun* 2017 81 8: 1–13
- Pardi N, Muramatsu H, Weissman D & Karikó K (2013) In vitro transcription of long RNA containing modified nucleosides. *Methods Mol Biol*
- Percharde M, Lin CJ, Yin Y, Guan J, Peixoto GA, Bulut-Karslioglu A, Biechele S, Huang B, Shen X & Ramalho-Santos M (2018) A LINE1-Nucleolin Partnership Regulates Early Development and ESC Identity. *Cell*
- Rau A, Gallopin M, Celeux G & Jaffrézic F (2013) Data-based filtering for replicated high-throughput transcriptome sequencing experiments. *Bioinformatics* 29: 2146–2152
- Recknagel S, Bindl R, Brochhausen C, Göckelmann M, Wehner T, Schoengraf P, Huber-Lang M, Claes L & Ignatius A (2013) Systemic inflammation induced by a thoracic trauma alters the cellular composition of the early fracture callus. *J Trauma Acute Care Surg* 74: 531–537
- Reppe S, Refvem H, Gautvik VT, Olstad OK, Høvrind PI, Reinholt FP, Holden M, Frigessi A, Jemtland R & Gautvik KM (2010) Eight genes are highly associated with BMD variation in postmenopausal Caucasian women. *Bone*
- Ritschka B, Storer M, Mas A, Heinzmann F, Ortells MC, Morton JP, Sansom OJ, Zender L & Keyes WM (2017) The senescence-associated secretory phenotype induces cellular plasticity and tissue regeneration. *Genes Dev* 31: 172–183
- Roberts SJ & Ke HZ (2018) Anabolic Strategies to Augment Bone Fracture Healing. *Curr Osteoporos Rep* 16: 289–298
- Robinson MD, McCarthy DJ & Smyth GK (2010) edgeR: a Bioconductor package for differential expression analysis of digital gene expression data. *Bioinformatics* 26: 139–140

Schmidt-Bleek K, Schell H, Schulz N, Hoff P, Perka C, Buttgereit F, Volk HD, Lienau J & Duda GN (2012)

Inflammatory phase of bone healing initiates the regenerative healing cascade. *Cell Tissue Res* 347: 567–573

Sheng W, LaFleur MW, Nguyen TH, Chen S, Chakravarthy A, Conway JR, Li Y, Chen H, Yang H, Hsu P-H, et al (2018) LSD1 Ablation Stimulates Anti-tumor Immunity and Enables Checkpoint Blockade. *Cell* 174: 549–563.e19

Simon M, Van Meter M, Ablaeva J, Ke Z, Gonzalez RS, Taguchi T, De Cecco M, Leonova KI, Kogan V, Helfand SL, et al (2019) LINE1 Derepression in Aged Wild-Type and SIRT6-Deficient Mice Drives Inflammation. *Cell Metab* 29: 871-885.e5

Slotkin RK & Martienssen R (2007) Transposable elements and the epigenetic regulation of the genome. *Nat Rev Genet* 8: 272–285

Strieter RM, Burdick MD, Gomperts BN, Belperio JA & Keane MP (2005) CXC chemokines in angiogenesis. *Cytokine Growth Factor Rev* 16: 593–609

Timmen M, Hidding H, Wieskötter B, Baum W, Pap T, Raschke MJ, Schett G, Zwerina J & Stange R (2014) Influence of antiTNF-alpha antibody treatment on fracture healing under chronic inflammation. *BMC Musculoskelet Disord* 15: 184

Della Valle F, Reddy P, Yamamoto M, Liu P, Saera-Vila A, Bensaddek D, Zhang H, Prieto Martinez J, Abassi L, Celii M, et al (2022) LINE-1 RNA causes heterochromatin erosion and is a target for amelioration of senescent phenotypes in progeroid syndromes. *Sci Transl Med* 14: eabl6057

Varanasi SS, Olstad OK, Swan DC, Sanderson P, Gautvik VT, Reppe S, Francis RM, Gautvik KM & Datta HK (2010) Skeletal Site-Related Variation in Human Trabecular Bone Transcriptome and Signaling. *PLoS One* 5: e10692

Wang S, Lee C, Kim J, Hyun J, Lim M, Cha H-J, Oh S-H, Choi YH & Jung Y (2017) Tumor necrosis factor-inducible gene 6 protein ameliorates chronic liver damage by promoting autophagy formation in mice. *Exp Mol Med* 49: e380

Weckbach S, Hohmann C, Braumueller S, Denk S, Klohs B, Stahel PF, Gebhard F, Huber-Lang MS & Perl M (2013) Inflammatory and apoptotic alterations in serum and injured tissue after experimental polytrauma in

- mice: distinct early response compared with single trauma or ‘double-hit’ injury. *J Trauma Acute Care Surg* 74: 489–498
- Wheatley BM, Nappo KE, Christensen DL, Holman AM, Brooks DI & Potter BK (2019) Effect of NSAIDs on Bone Healing Rates. *J Am Acad Orthop Surg* 27: e330–e336
- Wiśniewski JR, Zougman A, Nagaraj N & Mann M (2009) Universal sample preparation method for proteome analysis. *Nat Methods* 6: 359–362
- Xiao G, Gopalakrishnan R, Jiang D, Reith E, Benson MD & Franceschi RT (2002a) Bone morphogenetic proteins, extracellular matrix, and mitogen-activated protein kinase signaling pathways are required for osteoblast-specific gene expression and differentiation in MC3T3-E1 cells. *J Bone Miner Res* 17: 101–110
- Xiao G, Jiang D, Gopalakrishnan R & Franceschi RT (2002b) Fibroblast growth factor 2 induction of the osteocalcin gene requires MAPK activity and phosphorylation of the osteoblast transcription factor, Cbfa1/Runx2. *J Biol Chem* 277: 36181–36187
- Xiao G, Jiang D, Thomas P, Benson MD, Guan K, Karsenty G & Franceschi RT (2000) MAPK Pathways Activate and Phosphorylate the Osteoblast-specific Transcription Factor, Cbfa1 *. *J Biol Chem* 275: 4453–4459
- Yang A, Lu Y, Xing J, Li Z, Yin X, Dou C, Dong S, Luo F, Xie Z, Hou T, et al (2018a) IL-8 Enhances Therapeutic Effects of BMSCs on Bone Regeneration via CXCR2-Mediated PI3k/Akt Signaling Pathway. *Cell Physiol Biochem* 48: 361–370
- Yang H, Tian W, Wang S, Liu X, Wang Z, Hou L, Ge J, Zhang X, He Z & Wang X (2018b) TSG-6 secreted by bone marrow mesenchymal stem cells attenuates intervertebral disc degeneration by inhibiting the TLR2/NF-κB signaling pathway. *Lab Investig* 98: 755–772
- Yang WR, Ardeljan D, Pacyna CN, Payer LM & Burns KH (2019) SQuIRE reveals locus-specific regulation of interspersed repeat expression. *Nucleic Acids Res* 47: e27–e27
- Zhang R, Liu Y, Yan K, Chen L, Chen X-R, Li P, Chen F-F & Jiang X-D (2013) Anti-inflammatory and immunomodulatory mechanisms of mesenchymal stem cell transplantation in experimental traumatic brain injury. *J Neuroinflammation* 10: 106
- Zhang X, Zhang R & Yu J (2020) New Understanding of the Relevant Role of LINE-1 Retrotransposition in Human Disease and Immune Modulation. *Front cell Dev Biol* 8: 657
- Zhu W, Kuo D, Nathanson J, Satoh A, Pao GM, Yeo GW, Bryant S V., Voss SR, Gardiner DM & Hunter T (2012)

Retrotransposon long interspersed nucleotide element-1 (LINE-1) is activated during salamander limb regeneration. *Dev Growth Differ* 54: 673–685

Figure Legends

Figure 1 - TEs expression is induced after fracture and in mechanically loaded bone.

A) Heatmap representation of RNAseq differentially expressed TEs (LogFC>0.5) between 4h post-injury and intact femurs at different time points of the bone healing process. N=5 biological replicates for each time point. N=10 biological replicates for intact femur. **B)** Heatmap representation of RNAseq upregulated TEs (LogFC>0.5) between 4h and intact at different time points of the bone healing process. N=5 biological replicates for each time point. N=10 biological replicates for intact femur. **C)** Heatmap representation of RNAseq differentially expressed TEs analysis [Fragments Per Kilobase of transcript per Million (FPKM) fold change] in femoral (n=27) and iliac (n=34) bone biopsies from healthy donors. **D)** Pie charts showing the number and percentage of differentially expressed TEs subfamilies between femoral and iliac healthy bone. **E)** Heatmap representation of RNAseq differentially expressed TEs analysis [Fragments Per Kilobase of transcript per Million (FPKM) fold change] in femoral (n=27) and iliac (n=34) bone biopsies from healthy donors. One heatmap for each TEs order is shown.

Figure 2 - TEs expression correlates with bone mineral density in human weight-bearing bone.

A) Heatmap representation of RNAseq differentially expressed TEs analysis [Fragments Per Kilobase of transcript per Million (FPKM) fold change] in femoral bone from healthy (n=27), osteopenic (n=12), and osteoporotic (n=9) donors. **B)** Heatmap representation of RNAseq differentially expressed TEs analysis [Fragments Per Kilobase of transcript per Million (FPKM) fold change] in femoral bone with high BMD (FN T-score >-1) (n=27) and low BMD (FN T-score <-1) (n=21). **C)** Upper panels: pie charts showing the number and percentage of differentially expressed TEs subfamilies between high BMD and low BMD femoral bone. Lower panels: heatmap representation of RNAseq differentially expressed TEs analysis [Fragments Per Kilobase of transcript per Million (FPKM) fold change] in femoral bone with high BMD (n=27) and low BMD (n=21). One heatmap for each TEs order is shown. **D)** Upper panels: Heatmap representation of correlation analysis (P value<0.05) between TEs expression (FPKM) and local BMD (FN T-score) in femoral bone biopsies (n=48). Correlation between TE expression (FPKM values) and FN t-score was evaluated using Pearson method. Significant correlations (p -value < 0.05) were selected for the heatmap representation and arranged according to the Pearson correlation coefficient (r). $r > 0$, positive correlations;

$r < 0$, negative correlations. Lower panels: Pie charts showing the percentage of TEs subfamilies positively correlated to local BMD.

Figure 3 - L1 RNA delivery stimulates the mineralization of differentiating osteoblasts

A) Experimental workflow and flow cytometer analysis showing the percentage of positive cells 6 hours after L1 RNA delivery at day 5 of *ex vivo* osteogenesis. Intracellular localization of cy5 conjugated synthetic L1 RNA (red spots) three days after transfection is also shown from a typical experiment (right). **B)** qPCR analysis of intracellular L1 RNA level 24 h (d6), 5 days (d10), and 9 days (d14) post-transfection. The graph is shown as mean \pm s.d. of $n=3$ independent experiments. **C)** cy5 conjugated synthetic L1 RNA (red) and osteoimage stained mineral matrix (green) detection 9 days post L1 RNA transfection. The white arrowheads indicate the colocalization between L1 RNA and hydroxyapatite. **D)** Osteoimage stained mineral matrix quantification (upper panels), images (central panels), and Alizarin Red (lower panels) 9 days after L1 RNA or RFP RNA delivery in 2 healthy donors-derived MSCs (D188 and D170). RFU= Relative Fluorescence Units. The graph is shown as mean \pm s.d. of $n=11$ technical replicates. ***P<0.00005 in Wilcoxon test. **E)** Alizarin Red staining of osteoblasts transfected with increasing doses of RFP RNA (upper panels) and L1 RNA (lower panels). **F)** Alizarin Red images (upper panel) and quantification (lower panel) of MSCs mineralization after 14, 17 and 21 days of *ex vivo* differentiation. MSCs were obtained from the femur of 4 healthy (D188, D239, D247, D170) and 4 OP patients (HUK7, HUK9, HUK12, HUK16). N=9 technical replicates for each donor and time point. Boxes in the boxplot indicate the interquartile range (50% of data), while the lower end and the upper end represent the 1st and the 3rd quartile, respectively. The solid line inside the box represents the median. Whiskers represent the max and min values. Values that are not within 1.5 times the interquartile range are considered as outliers and lie outside the whiskers. **G)** Osteoimage stained mineral matrix quantification (upper panels), images (central panels), and Alizarin Red (lower panels) 9 days after L1 RNA or RFP RNA delivery in 3 OP patients derived MSCs (HUK9, HUK12, HUK16). RFU= Relative Fluorescence Units. The graph is shown as mean \pm s.d. of $n=10-12$ technical replicates. ***P<0.00005 in Wilcoxon test. **H)** qRT-PCR of early osteogenic genes in RFP and L1 transfected osteoblasts at different time points of osteogenic differentiation. Expression level is normalized on day 5 (not transfected osteoblasts). N=3 biological replicates. The graph is shown as mean \pm s.d. of $n=3$ independent experiments. *P<0.05; **P<0.005, ***P<0.0005, ****P<0.00005 in Student's t test.

Figure 4 - L1 RNA delivery induces an inflammatory response characteristic of bone repair process

A) Left panel: heatmap representation of RNAseq differentially expressed gene analysis [Fragments Per Kilobase of transcript per Million (FPKM) fold change] in osteoblasts transfected with negative control RNA (RFP) or L1 RNA. Right panel: bubble plot showing gene ontology (GO) enrichment analysis of L1 upregulated biological processes.

B) Tree plot showing gene ontology (GO) enrichment analysis of L1 upregulated biological processes (left) and cellular components (right). **C)** Top 25 upregulated biological processes 24h post-L1 RNA delivery *in vitro* (yellow) and 4h post fracture *in vivo* (blue). Shared GO terms are shown in green. **D)** qPCR analysis of “inflammatory response” (GO:0006954) and “immune response” (GO:0006955) genes at different time points post L1 RNA transfection at day 5. * **P < 0.005, ****P < 0.00005 in two way ANOVA.

Figure 5 - PKR mediates L1 RNA-induced stress response and mineralization

A) Upper panel: schematic representation of the pathway inhibited by Lamivudine 3TC and G140. Lower panel: Alizarin Red staining of differentiating osteoblasts transfected with L1 RNA and treated with Lamivudine 3TC and G140. **B)** IF on RFP and L1 transfected osteoblasts, 6h post-transfection, shows the colocalization between cy5 signal (L1 RNA, red) and 488-Anti-dsRNA signal (dsRNA, green). Nuclei are stained with Hoechst (blue).

C) Western blot analysis showing the ratio between total eIF2 α and phosphorylated eIF2 α (P- eIF2 α). H3: endogenous standard Histone 3. **D)** Volcano plot (left) showing the number of significantly upregulated and downregulated protein 24h post-L1 RNA transfection. Right: tree plots showing gene ontology (GO) enrichment analysis of biological processes (upper panel) and cellular components (lower panel) downregulated by L1 RNA delivery (MS data). **E)** qPCR analysis of “inflammatory response” (GO:0006954) and “immune response” (GO:0006955) genes 24h post L1 RNA transfection with and without PKR inhibitor C16. **F)** Alizarin Red staining of differentiating osteoblasts transfected with L1 RNA with and without PKR inhibitor C16. **G)** Tree plots showing gene ontology (GO) enrichment analysis of biological processes upregulated by L1 RNA 24h after transfection (MS data).

Figure 6 - L1-RNA-induced changes in osteoblast secretome

A) Left: Alizarin red staining on recipient OB 9 days after the delivery of conditioned media. Right: Microscope images of recipient OB 24h from the delivery of conditioned media. Mineralized nodules in OB receiving conditioned media from L1 treated OB are shown (orange arrows). **B)** Heat map of differentially expressed proteins in bulk secretome and exosomes derived from untransfected (NT), RFP- and L1-transfected osteoblasts. N=3 biological replicates. **C)** GO enrichment analysis of differentially expressed protein (adjusted p-value <0.05) in the

bulk secretome of L1 compared to RFP transfected osteoblasts. **D)** GO enrichment analysis of differentially expressed protein (adjusted p-value <0.05) in the exosomes of L1 compared to RFP transfected osteoblasts.

Figure 1

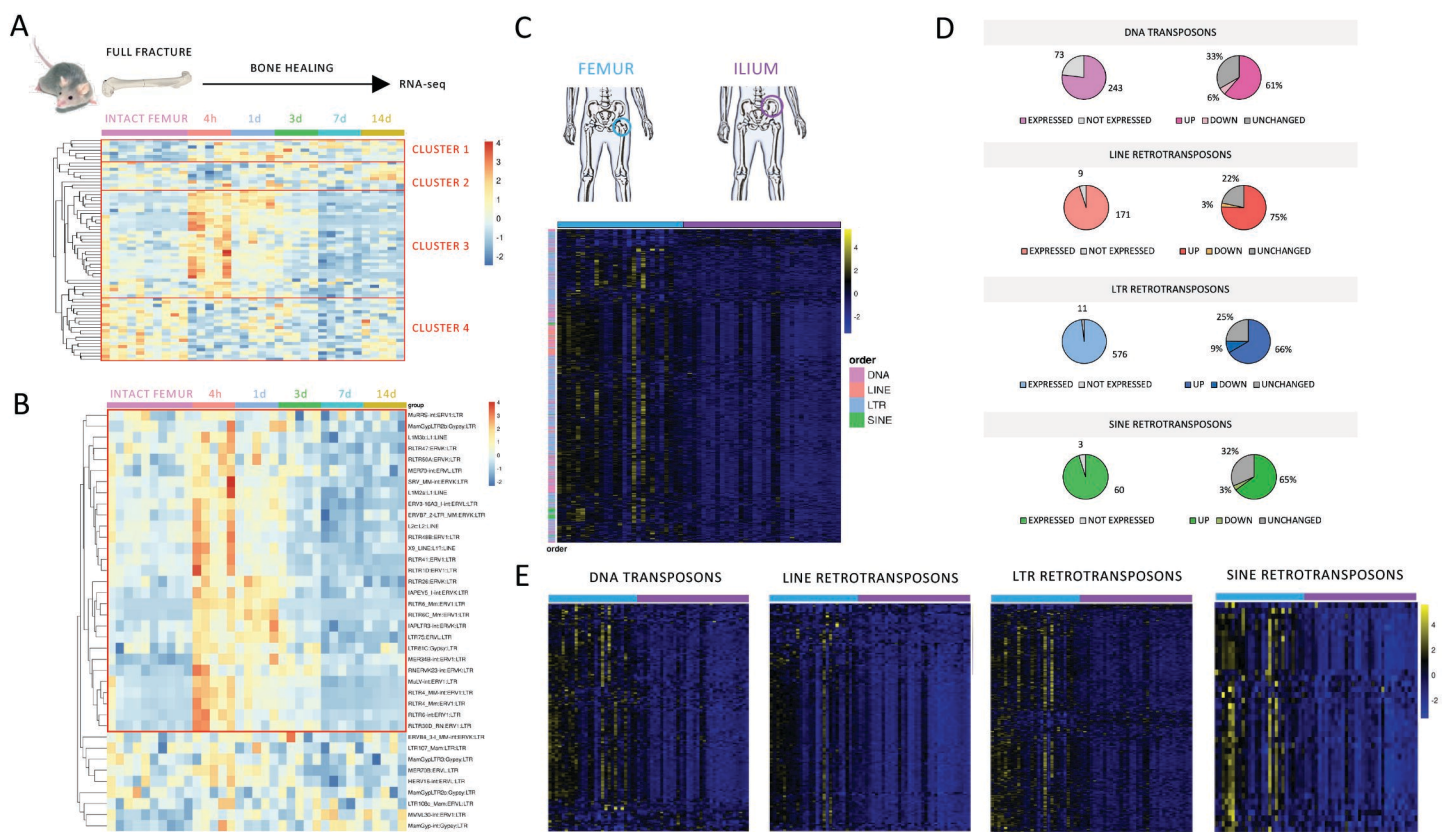


Figure 2

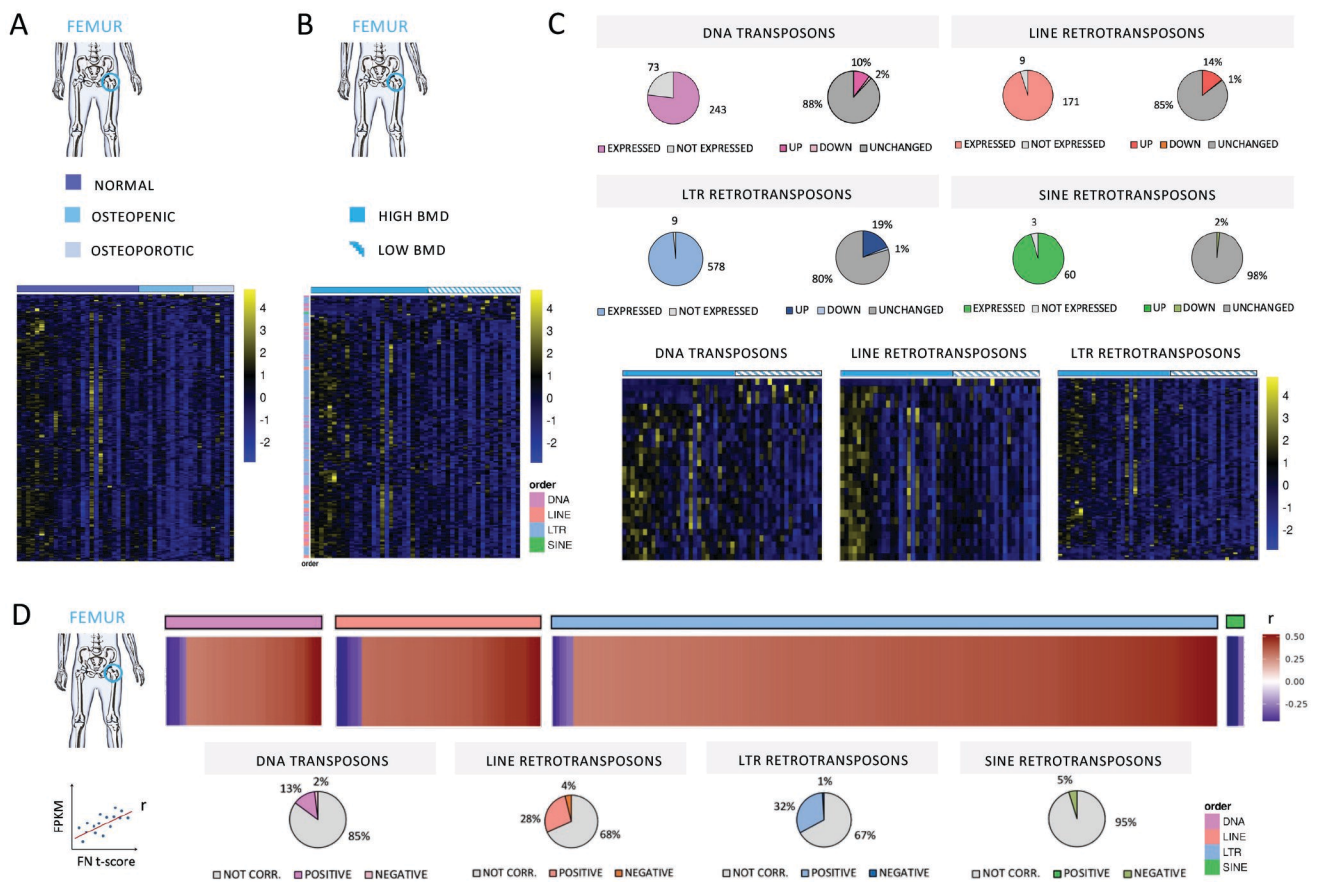


Figure 3

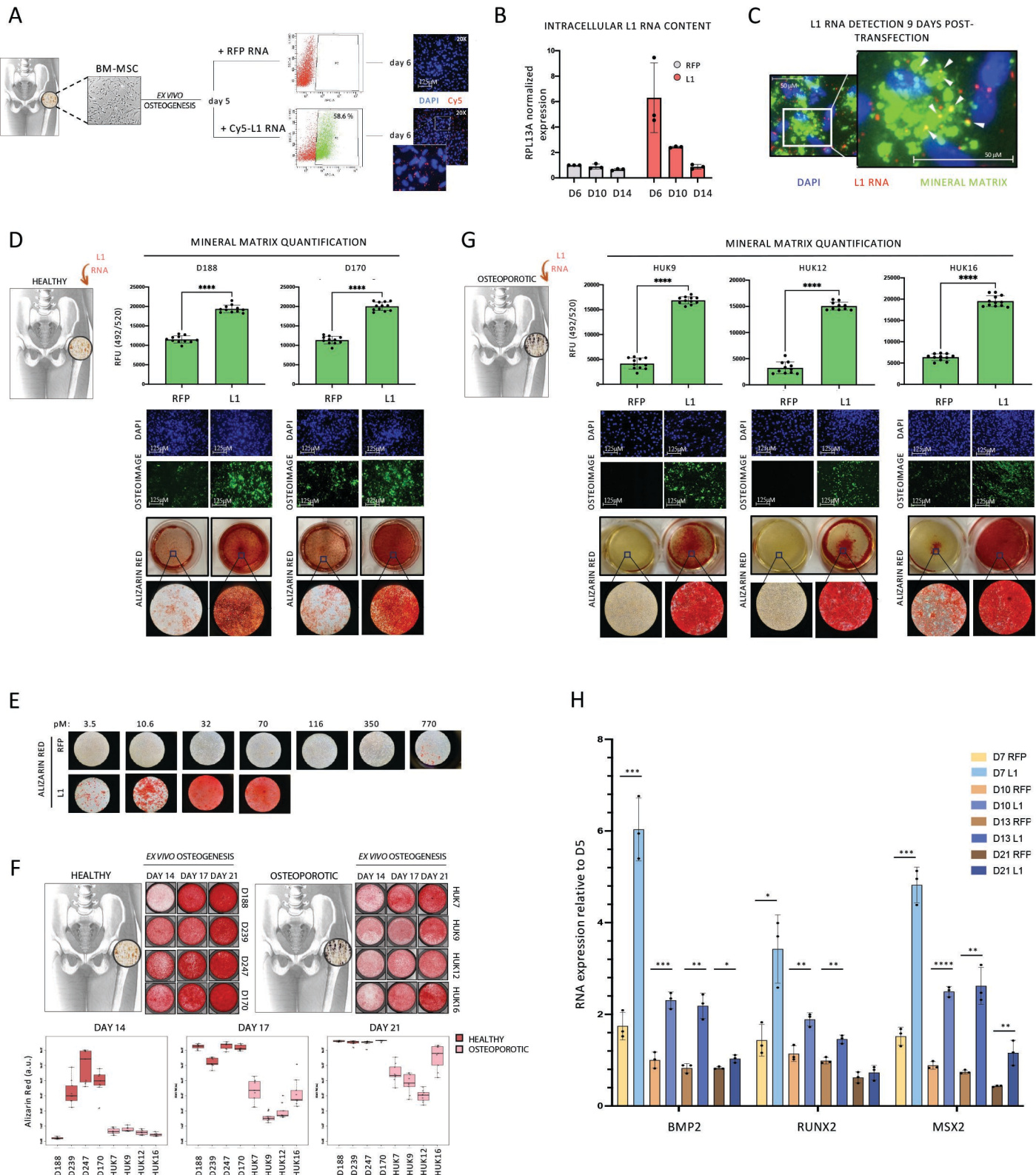


Figure 4

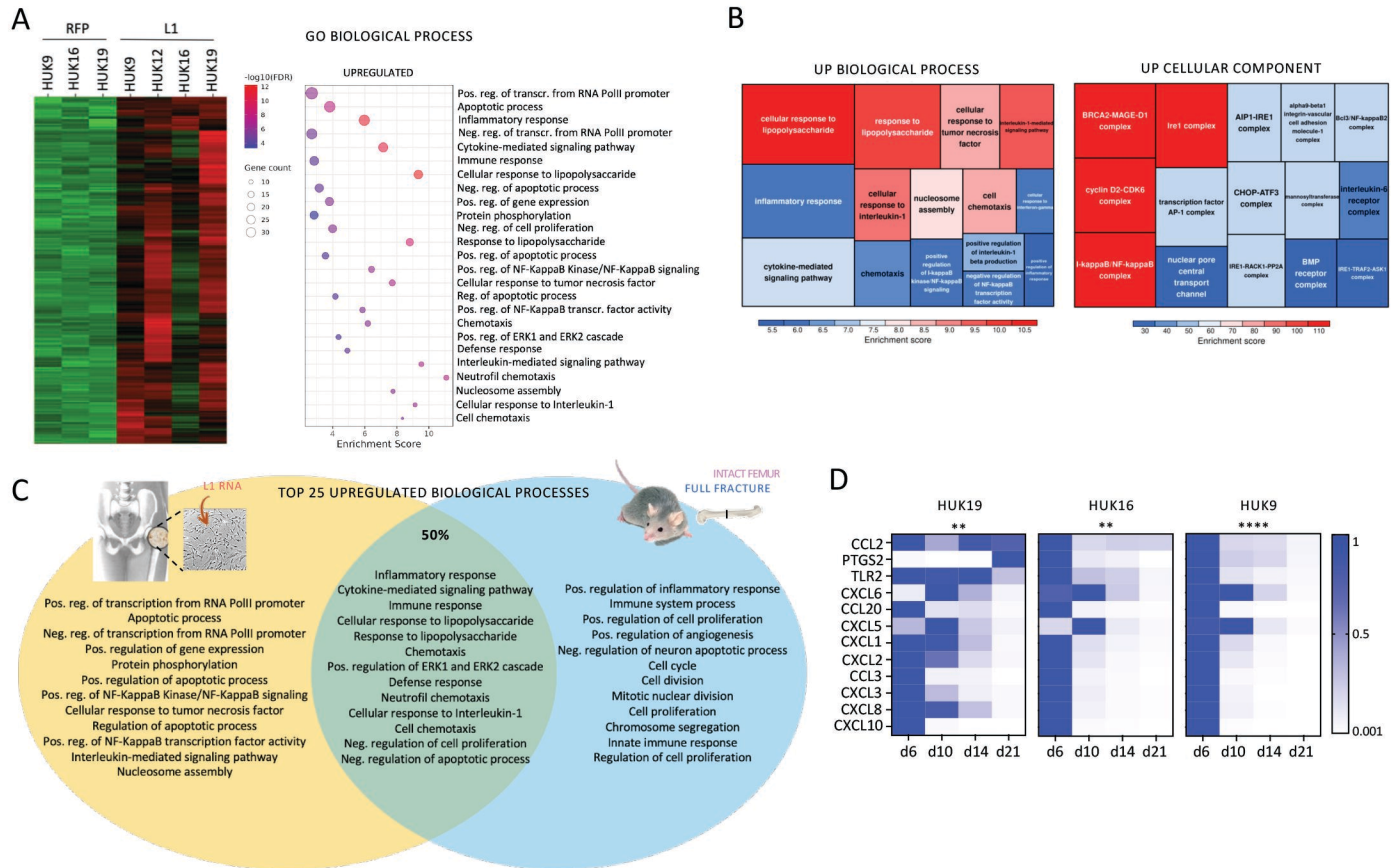


Figure 5

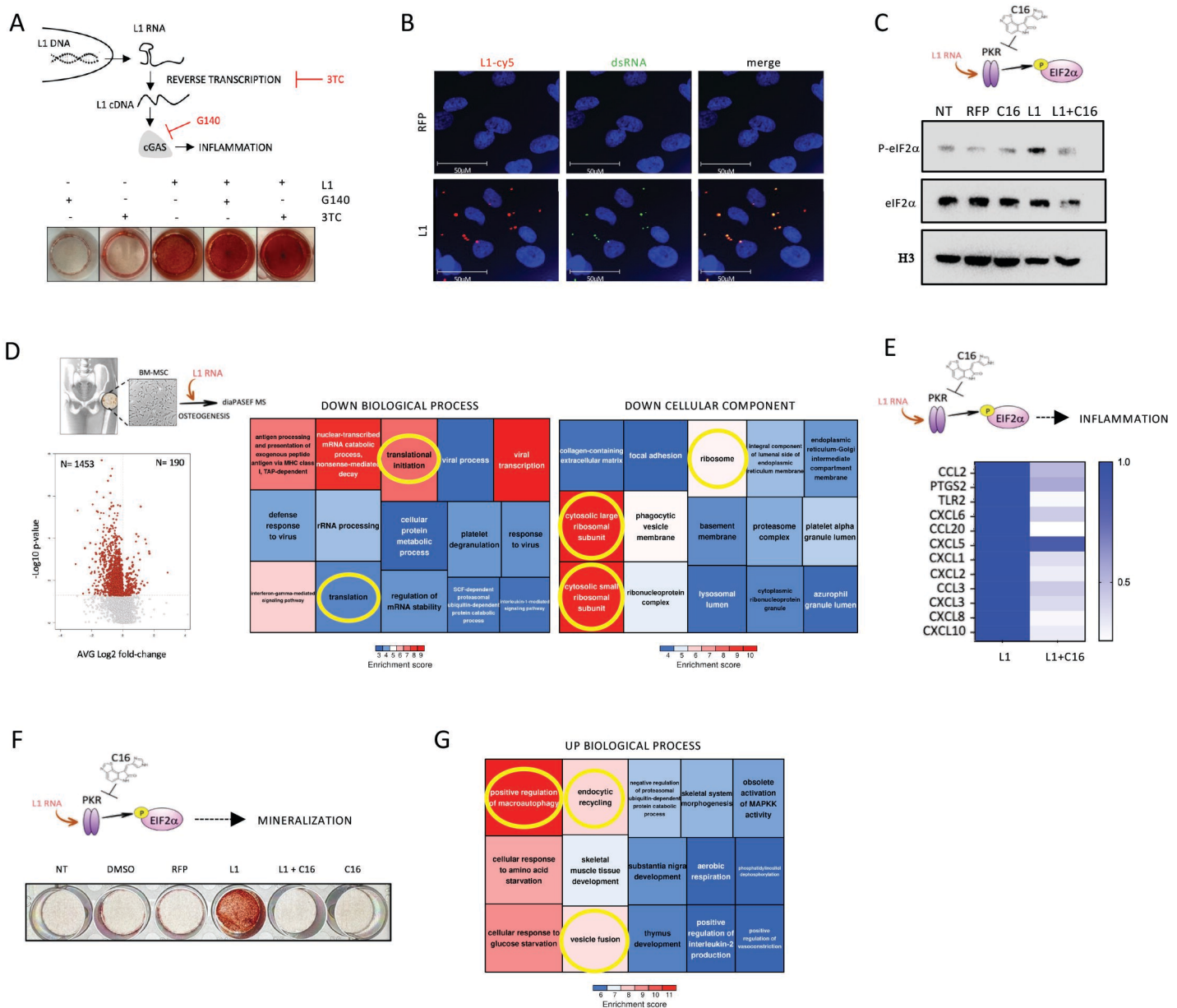


Figure 6

